EUROPEAN CENTRE FOR MEDIUM RANGE WEATHER FORECASTS

TECHNICAL REPORT NO. 11
****

APRIL

1979
****

NORMAL MODE INITIALIZATION FOR A MULTI-LEVEL GRIDPOINT MODEL

By

Clive Temperton
David L. Williamson*

European Centre for Medium Range Weather Forecasts

*On leave from the National Center for Atmospheric Research, which is sponsored by the National Science Foundation.

ABSTRACT

The normal modes of a linearized version of the ECMWF grid point global forecast model are determined and described. These modes are used for tests of the linear and non-linear normal mode initialization procedures when mountains are included in the model. The linear procedure is shown to have some problems which are alleviated by the non-linear correction procedure. The nonlinear iterative procedure converges to a good initial state when up to the first five vertical modes are initialized in the 9-level adiabatic frictionless model. When all nine vertical modes are included, the procedure diverges. The choice of the mean state which determines the normal modes is not crucial to the procedure. The nonlinear modal initialization is shown to be superior to dynamic initialization in terms of both computer time and elimination of unnatural oscillations in the forecast. The effect of including friction and physical parameterization in the model during the nonlinear iterations is discussed. The inclusion of the procedure in an analysis-initialization-forecast cycle is also described. In such a cycle the global rms changes made to the analysis by the initialization are no larger than observational errors.

1. Introduction

Since the introduction of primitive-equation models for numerical weather prediction, a completely satisfactory solution to the problem of defining an initial model state has proved elusive. Unless the initial mass and wind fields are carefully balanced, the forecast will be contaminated by inertia-gravity oscillations with amplitudes much greater than are observed in the atmosphere. The required balance is quite subtle, and the problem of satisfying it has been the subject of much research. Bengtsson (1975) has reviewed the initialization problem, and some of the methods which have been used in attempting to obtain balanced initial conditions.

It is sometimes argued that the spurious oscillations are relatively harmless, especially for forecasts of 12 - 24 hours or longer; that they can simply be removed by dissipation and/or damping time-integration schemes. Certainly in an adiabatic barotropic model they do not appear to interact with the meteorologically significant solution (Williamson, 1976). On the other hand the oscillations can be global in scale, with periods of several hours (e.g. Bourke, 1974), in which case the dissipation mechanisms will act rather slowly. In a multi-level model including good approximations to such highly nonlinear processes as precipitation and latent heat release, it is not clear that the forecast will be insensitive to unrealistic oscillations during the first few hours - particularly perhaps in the tropics, where there is a strong interaction between non-adiabatic processes and dynamics.

Furthermore, in the context of a data assimilation scheme based on an analysis/forecast cycle, in which a short forecast provides the first-guess fields for the next analysis, it is clearly important that these forecast fields should not be contaminated by spurious oscillations. With a cycle time as short as six hours, ad hoc damping mechanisms may not have sufficient time to be effective. If the oscillations can be removed before the start of the forecast, this should result in an improvement to the first-guess fields for the next analysis, and hence to the analysis itself, particularly in data-sparse regions.

Diagnostic initialization methods based on variants of the balance equation (e.g. Houghton and Washington,1969) have a number of disadvantages. In order to apply the balance equation to global models it is necessary to assume that the mass field determines the wind field in middle and high latitudes, and vice versa in the tropics; much of the analysed information is thereby discarded unless a variational approach (Stephens, 1970) is adopted. In mid-latitudes the analysed height fields sometimes have to be artificially modified in order to make the non-linear balance equation elliptic. The form of the balance equation must be carefully chosen to be consistent with the model's finite-difference scheme (Benwell and Bretherton,1968). Finally the balance equation only provides the rotational component of the wind field; Phillips (1960) showed that a consistent divergent component must also be included in order to suppress inertia-gravity oscillations. A global divergent component consistent with quasi-geostrophic theory can be obtained from the diagnostic ω-equation (Houghton et al., 1971); but despite the use of elaborate diagnostic initialization schemes, primitive-equation models continued to exhibit unrealistic oscillations.

An alternative approach, dynamic initialization, was suggested by Miyakoda and Moyer (1968) and Nitta and Hovermale (1969). In this approach the model's own prediction equations are used to integrate in a forward/backward cycle, using a time-integration scheme chosen to damp selectively the high-frequency oscillations. Mutual adjustment can take place between mass and wind fields. Temperton (1976) tested such a method on a hemispheric five-level model, and showed that it was quite successful in removing at least the external mode inertia-gravity oscillations with the highest frequencies. However, as the damping is purely frequency-dependent, dynamic initialization is unable to distinguish between large-scale inertia-gravity modes and small-scale Rossby modes. As in the case of diagnostic initialization, it is also difficult to incorporate the effects of physical parameterizations, some of which - particularly friction in the boundary layer - should influence the initial balance. Moreover, dynamic initialization is computationally expensive.

Recently normal mode initialization schemes have been developed, based on the fact that the eigenfunctions of the linearized primitive equations can be classified into inertia-gravity and Rossby wave solutions. Flattery (1970) based his Hough function analysis scheme on the normal modes of the linearized shallow-water equations (in continuous form) for a particular equivalent depth. Dickinson and Williamson (1972) showed how the normal modes of a linearized finite-difference forecast model could be obtained, and suggested an initialization procedure in which the initial data are projected onto the normal modes, the coefficients of unwanted modes are set to zero, and balanced initial fields are reconstituted from the remaining modes. In a purely linear forecast model, the amplitudes of the

unwanted modes would then remain zero. This procedure is somewhat analogous to solving the linear balance equation, except that a divergent component is also produced (due to the β-effect), and the mass and wind fields are mutually adjusted in a scale-dependent fashion consistent with geostrophic adjustment theory.

Williamson (1976) tested such an initialization scheme on a global barotropic model. He showed that although the amplitudes of the spurious oscillations were reduced, they were still to a significant extent regenerated by non-linear interactions. A further interesting result from this study was that a very similar 24-hour forecast was obtained if the initialization procedure was applied to the final forecast fields rather than to the initial fields, indicating that for this simple model the modes removed from the initial data (in the initialized case) did not interact significantly with the remaining modes during the 24-hour forecast if they were retained.

Machenhauer (1977), investigating the dynamics of gravity-mode oscillations in a barotropic spectral model, noticed that the contributions from nonlinear terms to the time tendencies of individual gravity mode coefficients oscillated about very slowly varying values. Based on this observation, he suggested that the oscillations could be removed from a forecast by setting to zero the initial time tendencies of the gravity mode coefficients, rather than the coefficients themselves. Machenhauer proposed an iterative scheme for accomplishing this, and demonstrated that it was highly successful in eliminating the spurious oscillations. Approaching the problem from a different viewpoint, Baer (1977) and Baer and Tribbia (1977) suggested a closely related procedure in which the initial time tendencies of the gravity modes are set to be the same order as those of the Rossby modes.

In Machenhauer's initialization scheme, the Rossby mode coefficients determined from the original data are left unaltered, while the gravity mode coefficients are adjusted in such a way that the linear contribution to the initial time derivative of each coefficient (which depends only on the coefficient itself) exactly balances the contribution from the nonlinear interactions between all the modes (Rossby and gravity). The adjustment is thus "forced" by the model's nonlinear terms.

Any initialization scheme may force larger changes to the analysed fields than would be compatible with the expected analysis error. Daley (1978) suggested a variational extension of Machenhauer's procedure, in which the initial time tendencies of the gravity mode coefficients are set to zero, while the changes to the original analysis are minimized. Daley successfully tested this variational procedure in a barotropic spectral model, under the highly idealized assumption that the expected analysis error for each variable was simply a function of latitude.

Andersen (1977) and Daley (1979) have extended Machenhauer's initialization scheme to multi-level models, with very encouraging results. In both cases the model used a spectral representation in the horizontal, and σ-coordinates in the vertical (though the vertical discretization was by finite differences in Andersen's model, and by finite elements in Daley's).

In this report we apply first linear and then nonlinear normal mode initialization to a multi-level model with a finite-difference representation in the horizontal. We show that the nonlinear procedure suggested by Machenhauer (1977) is highly successful in eliminating unwanted gravity-mode oscillations from forecasts made with such a model; moreover, it is economical in terms of computer

time. We also demonstrate its effectiveness within the context of a data assimilation scheme.

In the following section we present the analysis which is fundamental to the nonlinear normal mode initialization of the ECMWF gridpoint model. In Section 3 we briefly describe the normal modes of this model. Sections 4 and 5 present the results of linear and nonlinear initialization respectively, with the adiabatic version of the model. The effect of including surface drag is discussed in Section 6 and of including the complete physical parameterization in Section 7. The results of including the initialization procedure in a forecast-analysis cycle are presented in Section 8. Further applications are discussed briefly in Section 9.

2. Modal analysis

a. Vertical

In this section we present the analysis which is fundamental to the nonlinear normal mode initialization of the ECMWF grid point model. This analysis closely follows that of Machenhauer (1977) and Andersen (1977) for spectral models but uses the grid point notation introduced earlier by Dickinson and Williamson (1972), Williamson and Dickinson (1976) and Temperton (1977).

The normal modes of the linearized model are found by separation of variables. We first define a variable whose derivative gives the horizontal pressure gradient in the horizontal equations of motion, then relate the time change of this variable to the horizontal divergence. This relationship allows separation of the vertical variation and results in the shallow-water equations for

the horizontal variation of each vertical mode. These shallow-water equations have a different mean depth for each vertical mode. The global shallow-water equations are transformed by Fourier analysis to a problem involving only time and latitude which can be put into standard eigenvalue form. The eigenvalues are related to the frequencies of the normal modes and the eigenvectors to the latitudinal structure of the modes.

For the modal analysis, we explicitly include the terms of the equations linearized about a hydrostatic mean state at rest which is a function of σ, combining all the nonlinear terms in each equation into one term so that the horizontal equations of motion are written

$$\frac{\partial u_n}{\partial t} - fv_n + \frac{1}{a\cos\theta}\frac{\partial}{\partial\lambda}\overline{\phi}^{\sigma}_n + \frac{R\overline{T}_n}{a\cos\theta}\frac{\partial \ell n p_s}{\partial\lambda} = Qu_n \qquad (2.1)$$

$$\frac{\partial v_n}{\partial t} + fu_n + \frac{1}{a}\frac{\partial}{\partial\theta}\overline{\phi}^{\sigma}_n + \frac{R\overline{T}_n}{a}\frac{\partial \ell n p_s}{\partial\theta} = Qv_n \qquad (2.2)$$

where we have discretized only the vertical variation. We will discuss the implications of the mean state when mountains are present in Section 4. Details of the nonlinear terms can be determined from the complete equations in Burridge and Haseler (1977). The subscript is the vertical grid index (the grid is shown in Fig. 2.1) and a vertical average is denoted by

$$\overline{\phi}^{\sigma}_n = \frac{1}{2}\left(\phi_{n+\frac{1}{2}} + \phi_{n-\frac{1}{2}}\right) \qquad (2.3)$$

The normal meteorological notation is used where u and v are the zonal and meridional wind velocities, ϕ is geopotential, p_s surface pressure, θ latitude, λ longitude, t time, and f the Coriolis parameter.

The mean state $\overline{T}_n$ is given as a function of σ , and Qu_n and Qv_n represent all the nonlinear terms not included in the left sides of (2.1) and (2.2).

The thermodynamic equation for the temperature T is

$$\frac{\partial T_n}{\partial t} - \frac{\kappa \overline{T}_n}{\sigma_n}\left(\sigma\overline{\frac{\partial \ell n p_s}{\partial t}} + \dot{\sigma}\right)_n^{\sigma} \overline{\frac{\dot{\sigma}\ \Delta_\sigma \overline{T}_n}{(\Delta_\sigma \sigma)_n}}^{\sigma} = Q^* T_n \qquad (2.4)$$

where, for energy consistency, Burridge and Haseler (1977) take

$$\frac{1}{\sigma_n} = \frac{\Delta_\sigma \ell n \sigma}{\Delta_\sigma \sigma} \qquad (2.5)$$

The vertical difference is denoted

$$\Delta_\sigma A_n = A_{n+\frac{1}{2}} - A_{n-\frac{1}{2}} \qquad (2.6)$$

Again the nonlinear terms are combined into one term $Q^* T_n$.

The vertically integrated (summed) continuity equation is

$$\sigma_{n+\frac{1}{2}} \frac{\partial \ell n\, p_s}{\partial t} + \dot{\sigma}_{n+\frac{1}{2}} = -\sum_{\ell=1}^{n} \delta_\ell\, (\Delta\sigma)_\ell + Q\dot{\sigma}_{n+\frac{1}{2}} \qquad (2.7)$$

which, when summed to the bottom of the atmosphere at n=N, becomes the surface pressure tendency equation,

$$\frac{\partial \ell n\, p_s}{\partial t} = -\sum_{\ell=1}^{N} \delta_\ell (\Delta_\sigma \sigma)_\ell + Qp_s \qquad (2.8)$$

In (2.7) and (2.8) the horizontal divergence is given by

$$\delta_n = \frac{1}{a\cos\theta} \left(\frac{\partial u}{\partial \lambda} + \frac{\partial v\cos\theta}{\partial \theta}\right)_n \tag{2.9}$$

An equation relating vertical velocity and horizontal divergence is obtained from (2.7) and (2.8)

$$\dot{\sigma}_{n+\frac{1}{2}} = \sigma_{n+\frac{1}{2}} \sum_{\ell=1}^{N} \delta_\ell \, (\Delta_\sigma \sigma)_\ell - \sum_{\ell=1}^{n} \delta_\ell (\Delta_\sigma \sigma)_\ell$$

$$- \sigma_{n+\frac{1}{2}} Qp_s + Q\dot{\sigma}_{n+\frac{1}{2}} \tag{2.10}$$

Equations (2.7) and (2.10) can be combined with (2.4) to give a relation between T and δ which, in vector form, is written as

$$\frac{\partial \underset{\sim}{T}}{\partial t} + \underset{\sim}{\mathscr{T}} \underset{\sim}{\delta} = \underset{\sim}{Q}_T \tag{2.11}$$

where the vectors $\underset{\sim}{T}$, $\underset{\sim}{\delta}$, and $\underset{\sim}{Q}_T$ denote

$$\underset{\sim}{T} = \begin{pmatrix} T_1 \\ T_2 \\ \vdots \\ T_N \end{pmatrix}, \quad \underset{\sim}{\delta} = \begin{pmatrix} \delta_1 \\ \delta_2 \\ \vdots \\ \delta_N \end{pmatrix}, \quad \underset{\sim}{Q}_T = \begin{pmatrix} Q_{T_1} \\ Q_{T_2} \\ \vdots \\ Q_{T_N} \end{pmatrix} \tag{2.12}$$

and the matrix $\underset{\sim}{\mathscr{T}} = (\mathscr{T}_{n\ell})$ is given by

$$\mathcal{T}_{n\ell} = \begin{cases} \left[\dfrac{\kappa \overline{T}_n}{\sigma_n} - \dfrac{\frac{1}{2}(\overline{T}_{n+1} + \overline{T}_{n-1})}{(\Delta_\sigma \sigma)_n} + \tau_n \right] (\Delta_\sigma \sigma)_\ell & \text{for } \ell < n \\ \left[\frac{1}{2} \dfrac{\kappa \overline{T}_n}{\sigma_n} - \dfrac{\frac{1}{2}(\overline{T}_{n+1} - \overline{T}_n)}{(\Delta_\sigma \sigma)_n} + \tau_n \right] (\Delta_\sigma \sigma)_\ell & \text{for } \ell = n \\ \left[\tau_n \right] (\Delta_\sigma \sigma)_\ell & \text{for } \ell > n \end{cases} \tag{2.13}$$

$$\tau_n = \frac{\frac{1}{2}\left[\sigma_{n+\frac{1}{2}}(\overline{T}_{n+1} - \overline{T}_n) + \sigma_{n-\frac{1}{2}}(\overline{T}_n - \overline{T}_{n-1})\right]}{(\Delta_\sigma \sigma)_n}$$

In actual applications of (2.13) nonexisting values $\overline{T}_0$ and $\overline{T}_{N+1}$ are needed, however, any finite value can be inserted as the boundary conditions $\dot{\sigma} = 0$ at $\sigma = 0,1$ implicitly included in the derivation of (2.7) and (2.8) result in zero coefficients for $\overline{T}_0$ or $\overline{T}_{N+1}$. The nonlinear term of (2.11) is

$$Q_{T_n} = \frac{\kappa \overline{T}_n}{\sigma_n} \overline{\dot{Q}_\sigma}^{\sigma}_n + \frac{\Delta_\sigma \overline{T}_n (\sigma_{n+\frac{1}{2}} Qp_s - Q\dot{\sigma}_{n+\frac{1}{2}})}{\Delta_\sigma \sigma_n} + Q^*_{T_n} \tag{2.14}$$

The remaining equation needed for the vertical separation of variables is the vertically integrated (summed) hydrostatic equation

$$\phi_{n+\frac{1}{2}} = \phi_s + \sum_{\ell=n+1}^{N} RT_\ell \, (\Delta_\sigma \ell n \sigma)_\ell \tag{2.15}$$

The linearized equations can now be written in terms of vectors defined as in (2.12)

$$\frac{\partial \underset{\sim}{u}}{\partial t} - f\underset{\sim}{v} + \frac{1}{a\cos\theta}\frac{\partial}{\partial \lambda}\left(R\underset{\sim}{\overline{T}}\ell n p_s + \underset{\sim}{\overline{\phi}}^{\sigma}\right) = \underset{\sim}{Q}_u \tag{2.16}$$

$$\frac{\partial \underset{\sim}{v}}{\partial t} + f\underset{\sim}{u} + \frac{1}{a}\frac{\partial}{\partial \theta}\left(R\underset{\sim}{\overline{T}}\ell n p_s + \underset{\sim}{\overline{\phi}}^{\sigma}\right) = \underset{\sim}{Q}_v \tag{2.17}$$

$$\frac{\partial \underset{\sim}{T}}{\partial t} + \underset{\sim}{\mathscr{T}}\,\underset{\sim}{\delta} = \underset{\sim}{Q}_T \tag{2.18}$$

$$\frac{\partial \ell n p_s}{\partial t} + \underset{\sim}{\Pi}^T \underset{\sim}{\delta} = Qp_s \tag{2.19}$$

$$\underset{\sim}{\overline{\phi}}^{\sigma} = \underset{\sim}{\phi}_s + \underset{\sim\sim}{G}\underset{\sim}{T} \tag{2.20}$$

where the vector $\Pi_\ell = (\Delta_\sigma \sigma)_\ell$ and the superscript T denotes the transpose of a vector. The matrix $G = (G_{n\ell})$ is given by

$$\begin{aligned} G_{n\ell} &= 0 \text{ for } \ell < n \\ G_{n\ell} &= \tfrac{1}{2}R(\Delta_\sigma \ell n \sigma)_\ell \text{ for } \ell = n \\ G_{n\ell} &= R(\Delta_\sigma \ell n \sigma)_\ell \text{ for } \ell > n \end{aligned} \tag{2.21}$$

and the vector $\underset{\sim}{\phi}_s$ has ϕ_s for each entry.

To determine the vertical modes we define a vector $\underset{\sim}{h}$ whose horizontal derivative represents the horizontal pressure gradient force,

$$g\underset{\sim}{h} = \underset{\sim}{\bar{\phi}}^{\sigma} + R\underset{\sim}{\bar{T}}\ell n p_s \tag{2.22}$$

where g is gravity. Then, Equations (2.16)-(2.20) can be written

$$\frac{\partial \underset{\sim}{u}}{\partial t} - f\underset{\sim}{v} + \frac{g}{a\cos\theta}\frac{\partial \underset{\sim}{h}}{\partial \lambda} = \underset{\sim}{Q}_u \tag{2.23}$$

$$\frac{\partial \underset{\sim}{v}}{\partial t} + f\underset{\sim}{u} + \frac{g}{a}\frac{\partial \underset{\sim}{h}}{\partial \theta} = \underset{\sim}{Q}_v \tag{2.24}$$

$$g\frac{\partial \underset{\sim}{h}}{\partial t} = -\underset{\sim}{C}\,\underset{\sim}{\delta} + g\underset{\sim}{Q}_h \tag{2.25}$$

where

$$\underset{\sim}{C} = \underset{\sim}{G}\underset{\sim}{\mathscr{T}} + R\underset{\sim}{\bar{T}}\;\underset{\sim}{\Pi}^T \tag{2.26}$$

and

$$g\underset{\sim}{Q}_h = \underset{\sim}{G}\,\underset{\sim}{Q}_T + R\underset{\sim}{\bar{T}}\,Qp_s \tag{2.27}$$

Equations (2.23) and (2.24) represent equations at each vertical level with no coupling between levels, however (2.25) represents a coupled set of equations since, in general, $\underset{\sim}{C}$ has non-zero off-diagonal elements. In order to separate variables and determine the vertical structure of the normal modes, we employ the eigenvalues of $\underset{\sim}{C}$, denoted gD_m, and the corresponding eigenvectors, $\underset{\sim}{\Phi}_m$. Let $\underset{\sim}{\Phi}$ be the matrix whose columns are the eigenvectors of $\underset{\sim}{C}$,

$$\underset{\sim}{\Phi} = (\underset{\sim}{\Phi}_1\ \underset{\sim}{\Phi}_2 \cdots \underset{\sim}{\Phi}_M) \tag{2.28}$$

and $g\underset{\sim}{D}$ be the diagonal matrix of corresponding eigenvalues

$$g\underset{\sim}{D} = g \begin{bmatrix} D_1 & & & \\ & D_2 & & 0 \\ & & \ddots & \\ & 0 & & D_M \end{bmatrix} \tag{2.29}$$

so that

$$\underset{\sim}{C}\underset{\sim}{\phi} = \underset{\sim}{\phi} g\underset{\sim}{D} \tag{2.30}$$

or

$$\underset{\sim}{\phi}^{-1} \underset{\sim}{C}\underset{\sim}{\phi} = g\underset{\sim}{D} \tag{2.31}$$

Then the vertical transformation

$$\begin{aligned} \bar{\underset{\sim}{u}} &= \underset{\sim}{\phi}^{-1}\underset{\sim}{u} \quad , \quad \bar{\underset{\sim}{Q}}_u = \underset{\sim}{\phi}^{-1} \underset{\sim}{Q}_u \\ \bar{\underset{\sim}{v}} &= \underset{\sim}{\phi}^{-1}\underset{\sim}{v} \quad , \quad \bar{\underset{\sim}{Q}}_v = \underset{\sim}{\phi}^{-1} \underset{\sim}{Q}_v \\ \bar{\underset{\sim}{h}} &= \underset{\sim}{\phi}^{-1}\underset{\sim}{h} \quad , \quad \bar{\underset{\sim}{Q}}_h = \underset{\sim}{\phi}^{-1} \underset{\sim}{Q}_h \end{aligned} \tag{2.32}$$

gives

$$\frac{\partial \bar{\underset{\sim}{u}}}{\partial t} - f\bar{\underset{\sim}{v}} + \frac{g}{a\cos\theta} \frac{\partial \bar{\underset{\sim}{h}}}{\partial \lambda} = \bar{\underset{\sim}{Q}}_u \tag{2.33}$$

$$\frac{\partial \bar{\underset{\sim}{v}}}{\partial t} + f\bar{\underset{\sim}{u}} + \frac{g}{a} \frac{\partial \bar{\underset{\sim}{h}}}{\partial \theta} = \bar{\underset{\sim}{Q}}_v \tag{2.34}$$

$$\frac{\partial \bar{\underset{\sim}{h}}}{\partial t} + \underset{\sim}{D}\,\bar{\underset{\sim}{\delta}} = \bar{\underset{\sim}{Q}}_h \tag{2.35}$$

Since $\underset{\sim}{D}$ is diagonal, (2.33)-(2.35) represent an uncoupled system of equations for the coefficients of the vertical modes

$$\left.\begin{aligned}
&\frac{\partial \bar{u}_m}{\partial t} - f\bar{v}_m + \frac{g}{a\cos\theta}\frac{\partial \bar{h}_m}{\partial \lambda} = \bar{Q}u_m \\
&\frac{\partial \bar{v}_m}{\partial t} + f\bar{u}_m + \frac{g}{a}\frac{\partial \bar{h}_m}{\partial \theta} = \bar{Q}v_m \\
&\frac{\partial \bar{h}_m}{\partial t} + D_m\,\bar{\delta}_m = \bar{Q}h_m
\end{aligned}\right\} \quad m=1,..,M \qquad (2.36)$$

The eigenvectors $\underset{\sim}{\Phi}_m$ are referred to as the vertical modes and transformed variables $\bar{u}_m$, $\bar{v}_m$, $\bar{h}_m$, etc., as the coefficients of the m^{th} vertical mode since, from (2.32)

$$\underset{\sim}{u} = \underset{\sim}{\Phi}\,\underset{\sim}{\bar{u}} \qquad (2.37)$$

In terms of scalars this is just a summation over the vertical modes evaluated at the n^{th} level, as in (6.4) of Williamson and Dickinson (1976)

$$u_n = \sum_{m=1}^{M} \bar{u}_m \Phi_m(n) \qquad (2.38)$$

We will see in Sections 4 and 5 that to apply the initialization procedures the vertical mode coefficients from (2.32) are needed. Since, in general, the matrix $\underset{\sim}{C}$ is not symmetric, the eigenvectors $\underset{\sim}{\Phi}_m$ defining the matrix $\underset{\sim}{\Phi}$ are not in general orthogonal and the inverse needed in (2.32) must be found by standard matrix inversion procedures. This is not a serious problem as the order of the matrix involved is rather small. It does, however, eliminate the possibility of comparing the energies in various vertical modes by comparing their coefficients. The matrix $\underset{\sim}{C}$ is symmetric for equally-spaced σ-levels and an isothermal base atmosphere. In this case the eigenvectors are orthogonal and the inverse of $\underset{\sim}{\Phi}$ is just the transpose of $\underset{\sim}{\Phi}$.

We see from (2.33)-(2.35) that the coefficients of the m^{th} vertical mode satisfy the shallow water equations with mean depth given by D_m. We discuss the structure of the vertical modes in Section 3.

b. Horizontal

The details of the determination of the horizontal modes of the ECMWF model have been given by Temperton (1977). We review the general approach here to illustrate how they relate to Machenhauer's (1977) nonlinear correction procedure.

The shallow water equations (2.36) for the vertical coefficients must first be approximated with the particular difference approximations of the forecast model. These approximations are given for the ECMWF model in Section 3 of Temperton (1977). The longitudinal dependence is then separated by Fourier transformation of the variables and of the nonlinear terms.

Let $\bar{\underset{\sim}{\gamma}}$ denote the horizontal grid point values of the vertical mode coefficients

$$\bar{\underset{\sim}{\gamma}}(\lambda_i,\theta_j,m) = \begin{pmatrix} \bar{u}(\lambda_i,\theta_j,m) \\ \bar{v}(\lambda_i,\theta_j,m) \\ \bar{h}(\lambda_i,\theta_j,m) \end{pmatrix} \tag{2.39}$$

The expansion into Fourier modes is written

$$\bar{\underset{\sim}{\gamma}}(\lambda_i,\theta_j,m) = \sum_{k=0}^{I-1} \tilde{\underset{\sim}{\gamma}}(k,\theta_j,m)e^{ik\lambda_i} \tag{2.40}$$

where I is the number of points around a latitude circle. The

inverse is

$$\tilde{\underline{\gamma}}(k,\theta_j,m) = \frac{1}{I}\sum_{i=1}^{I} \bar{\underline{\gamma}}(\lambda_i,\theta_j,m)e^{-ik\lambda_i} \qquad (2.41)$$

The ECMWF finite-difference approximations to the shallow water equations (2.36) for the Fourier amplitudes are then of the form

$$\delta_t\tilde{u}_j - \frac{1}{\cos\theta_j}\frac{r(k)}{2}\{f_j^- \cos\theta_{j-\frac{1}{2}}\tilde{v}_{j-\frac{1}{2}} + f_j^+\cos\theta_{j+\frac{1}{2}}\tilde{v}_{j+\frac{1}{2}}\}$$

$$+ g\frac{ik'}{a\cos\theta_j}\tilde{h}_j = \tilde{Q}_u(\theta_j) \qquad (2.42)$$

$$\delta_t\tilde{v}_{j+\frac{1}{2}} + \frac{r(k)}{2}\{f_{j+1}^+ \tilde{u}_{j+1} + f_j^-\tilde{u}_j\}$$

$$+ \frac{g}{a\Delta\theta}(\tilde{h}_{j+1}-\tilde{h}_j) = \tilde{Q}_v(\theta_{j+\frac{1}{2}}) \qquad (2.43)$$

$$\delta_t\tilde{h}_j + \frac{D_m}{a\cos\theta_j}\left\{ik'u_j\right.$$

$$\left. + \frac{1}{\Delta\theta}\left[\tilde{v}_{j+\frac{1}{2}}\cos\theta_{j+\frac{1}{2}} - \tilde{v}_{j-\frac{1}{2}}\cos\theta_{j-\frac{1}{2}}\right]\right\} = \tilde{Q}_h(\theta_j) \qquad (2.44)$$

where

$$f_j^+ = (\cos\tfrac{1}{2}\Delta\theta)^{-1}(\tfrac{2}{3}f_{j+\frac{1}{2}} + \tfrac{1}{3}f_{j-\frac{1}{2}}) \qquad (2.45)$$

$$f_j^- = (\cos\tfrac{1}{2}\Delta\theta)^{-1}(\tfrac{1}{3}f_{j+\frac{1}{2}} + \tfrac{2}{3}f_{j-\frac{1}{2}}) \qquad (2.46)$$

The discrete variables are defined on a staggered grid with u between h points in the λ direction and v between h points in the θ direction, δ_t represents the time differencing operator, left general for now, r(k) is the response function

of the average operator in the λ direction

$$r(k) = \cos(\tfrac{1}{2}k\Delta\lambda) \tag{2.47}$$

and ik' is the response function of the difference operator in the λ direction

$$k' = (\sin\tfrac{1}{2}k\Delta\lambda)/(\tfrac{1}{2}\Delta\lambda) \tag{2.48}$$

The Fourier coefficients of the nonlinear terms are represented by $\tilde{Q}_u$, $\tilde{Q}_v$ and $\tilde{Q}_h$. In (2.42)-(2.44) we have dropped the Fourier mode index k and, except for D_m, the vertical mode index m.

Since the longitudinal average and difference of a Fourier mode result in the same mode but with modified amplitude and phase and since the coefficients in (2.42)-(2.44) are independent of longitude, the Fourier transform diagonalizes the longitudinal dependence (as the vertical modes did the vertical dependence) resulting in a separate problem for each Fourier mode (and each vertical mode).

Because of the coupling between adjacent latitudes by the difference and average operators, (2.42)-(2.44) represent a set of simultaneous equations for $\tilde{\underset{\sim}{Y}}_j = (\tilde{u}_j, \tilde{v}_j, \tilde{h}_j)^T$ as j varies from the north to south pole. Examination of the form of the equations shows that the solution can be written in terms of vectors with certain symmetry properties about the equator. Thus we can solve two smaller sets of simultaneous equations with j varying from the pole to the equator; one for the symmetric vectors in which u and h are symmetric about the equator and v is antisymmetric and the other for the antisymmetric vectors in which u and h are antisymmetric about the equator and v symmetric. In order to diagonalize these problems we first scale the

variables by

$$\tilde{\underset{\sim}{\gamma}}'_j = \underset{\sim}{S}_m \tilde{\underset{\sim}{\gamma}}_j \tag{2.49}$$

where

$$\underset{\sim}{S}_m = \begin{pmatrix} 1 & 0 & 0 \\ 0 & -i & 0 \\ 0 & 0 & (gD_m)^{-\frac{1}{2}} \end{pmatrix} \tag{2.50}$$

Similarly for the nonlinear terms. The imaginary i represents a $\pi/2$ phase shift of v with respect to u and h. If we let $\tilde{\underset{\sim}{\gamma}}'$ be the vector of length L of the unknown variables from equator to pole, $\tilde{\underset{\sim}{\gamma}}' = (\tilde{\underset{\sim}{\gamma}}'^T_1 \; \tilde{\underset{\sim}{\gamma}}'^T_2 \; \tilde{\underset{\sim}{\gamma}}'^T_j)^T$ the equations have the general form

$$-i\underset{\sim}{Q}\delta_t\tilde{\underset{\sim}{\gamma}}' + \underset{\sim}{L}\tilde{\underset{\sim}{\gamma}}' = -i\underset{\sim}{Q}\tilde{\underset{\sim}{H}}' \tag{2.51}$$

Details of the analysis to arrive at this equation are in Temperton (1977) for the ECMWF model and Williamson and Dickinson (1976) for the NCAR model. The vector $\tilde{\underset{\sim}{\gamma}}'$ represents the latitudinal variation of u, v, and h while $\tilde{\underset{\sim}{H}}'$ represents the latitudinal variation of the corresponding nonlinear terms transformed the same way u, v, and h are to give $\tilde{\underset{\sim}{\gamma}}'$. In (2.51) the time difference operator δ_t has not yet been specified resulting in a slightly different form of the equation than in Temperton (1977) or Williamson and Dickinson (1976). The matrix $\underset{\sim}{Q}$ is diagonal and positive definite with entries related to the $\cos\theta_j$, and $\underset{\sim}{L}$ is a matrix depending on the actual finite differences used in the model. In our case $\underset{\sim}{L}$ is symmetric.

Let

$$\hat{\underset{\sim}{\gamma}} = \underset{\sim}{Q}^{\frac{1}{2}}\tilde{\underset{\sim}{\gamma}}', \hat{\underset{\sim}{H}} = \underset{\sim}{Q}^{\frac{1}{2}}\tilde{\underset{\sim}{H}}', \; \hat{\underset{\sim}{L}} = \underset{\sim}{Q}^{-\frac{1}{2}}\underset{\sim}{L}\,\underset{\sim}{Q}^{-\frac{1}{2}} \tag{2.52}$$

so that

$$-i\delta_t\hat{\underset{\sim}{\gamma}} + \hat{\underset{\sim}{L}}\hat{\underset{\sim}{\gamma}} = i\hat{\underset{\sim}{H}} \tag{2.53}$$

We now proceed as we did in determining the vertical modes. Let $\hat{\underset{\sim}{Y}}$ be the matrix whose columns are the eigenvectors $\hat{\underset{\sim}{Y}}^{\ell}$ of $\hat{\underset{\sim}{L}}$ and let $\hat{\underset{\sim}{\Lambda}}$ be the diagonal matrix of corresponding eigenvalues ν'_{ℓ} .

$$\hat{\underset{\sim}{Y}}^{-1}\hat{\underset{\sim}{L}}\hat{\underset{\sim}{Y}} = \hat{\underset{\sim}{\Lambda}} \tag{2.54}$$

Equation (2.53) can be transformed to

$$\delta_t \hat{\underset{\sim}{Y}}^{-1}\hat{\underset{\sim}{\gamma}} = -i\hat{\underset{\sim}{\Lambda}}\hat{\underset{\sim}{Y}}^{-1}\hat{\underset{\sim}{\gamma}} + \hat{\underset{\sim}{Y}}^{-1}\underset{\sim}{H} \tag{2.55}$$

Since $\hat{\underset{\sim}{\Lambda}}$ is diagonal, this problem separates into L independent equations for the components of the vector $\hat{\underset{\sim}{Y}}^{-1}\hat{\underset{\sim}{\gamma}}$ which we denote by c(k,ℓ,m), i.e.

$$\hat{\underset{\sim}{Y}}^{-1}\hat{\underset{\sim}{\gamma}} = \underset{\sim}{c}(k,m) = \begin{pmatrix} c(k,1,m) \\ c(k,2,m) \\ \vdots \\ c(k,L,m) \end{pmatrix} \tag{2.56}$$

Note that since $\hat{\underset{\sim}{L}}$ is symmetric, $\hat{\underset{\sim}{Y}}^{-1} = \hat{\underset{\sim}{Y}}^{T}$ so that if we define $\underset{\sim}{Y} = \underset{\sim}{Q}^{-\frac{1}{2}}\hat{\underset{\sim}{Y}}$,

$$\underset{\sim}{c}(k,m) = \underset{\sim}{Y}^{T}\underset{\sim}{Q}\hat{\underset{\sim}{\gamma}}' \tag{2.57}$$

which is just the vector form of Equation (6.13) of Williamson and Dickinson (1976).

Since $\hat{\underset{\sim}{L}}$ is symmetric, its eigenvectors are orthogonal and the inverse of the matrix of eigenvectors is just the transpose ($\hat{\underset{\sim}{Y}}^{-1} = \hat{\underset{\sim}{Y}}^{T}$). Thus each coefficient c can be determined by a vector inner product of its corresponding vector with the grid point data (2.56) or (2.57). This orthogonality resulting from the symmetry of L is a very convenient property as the order of the matrix is fairly large and computing its inverse would at least double

the computer time needed over that to compute the vectors. Alternatively one could use the vectors of the transpose of $\hat{\underset{\sim}{L}}$ to give a biorthogonal set with those of $\hat{\underset{\sim}{L}}$, however this also doubles the computer time needed to determine the modes and doubles the storage needed for the two sets.

Because of the separation, (2.55) can be rewritten as

$$\delta_t c(k,\ell,m) = - i\nu' c(k,\ell,m) + r(k,\ell,m) \qquad (2.58)$$

where we denote the ℓ^{th} component of the nonlinear terms $\hat{\underset{\sim}{Y}}^{-1}\underset{\sim}{H} = \underset{\sim}{Y}^T\underset{\sim}{Q}\tilde{\underset{\sim}{H}}'$ by $r(k,\ell,m)$. We refer to $c(k,\ell,m)$ as the coefficient of the normal mode and $\underset{\sim}{Y}$ as the latitudinal normal mode because inverting (2.57) for the latitudinal grid point data gives

$$\underset{\sim}{\gamma}' = \underset{\sim}{Y}\underset{\sim}{c}(k,m) \qquad (2.59)$$

which in terms of the scalar grid point values is just a summation over the latitudinal modes evaluated at a particular latitude times the coefficient of that mode [see Equation (6.11) of Williamson and Dickinson (1976)]. We discuss these modes in the next section.

3. Normal modes of ECMWF grid point model

a. Vertical modes

The vertical modes are the eigenvectors of the matrix $\underset{\sim}{C}$ as discussed in Section 2. The matrix $\underset{\sim}{C}$ is specified by the assumed hydrostatic mean state and the location of the vertical levels in σ space. The σ levels in the version of the ECMWF model used for our experiments are given in Table 3.1. These values enter in the matrix $\underset{\sim}{C}$ along with the values of $1/\sigma$ from (2.5). This equation cannot be applied at the top layer since the nominal value of σ at the top is 0. Instead, an effective thickness of the upper level is specified in the model by $(1/\sigma)_1 = 1/(\sigma_1) = 112.1538$, and $\Delta_\sigma \ell n \sigma$ in Equation (2.21) is defined by means of Equation (2.5).

Each vertical mode or eigenvector has a corresponding equivalent depth or eigenvalue which represents the mean depth in the shallow-water equations (2.36) used to determine the horizontal modes associated with that vertical mode. Table 3.2 lists the equivalent depths for two different mean temperature distributions with the nine σ levels specified as above. One temperature distribution is the global average from 1 March 1965 given in Table 3.3, the other is isothermal 300 ^{o}K. The table also lists the phase speeds of the gravity waves on a non-rotating earth, $\sqrt{gD}$. The corresponding eigenvectors are shown in Figs. 3.1 and 3.2 plotted as a function of σ . These modes and equivalent depths can be compared with those from other models such as Hoskins and Simmons (1975), Williamson and Dickinson (1976), or Daley (1979). The first eigenvector corresponding to the largest equivalent depth represents the external mode having no sign change with height. The vector corresponding to the second largest depth has one sign change and is referred to as the first internal mode.

Each successively smaller equivalent depth has a corresponding vector with one additional sign change until the last internal mode with the smallest equivalent depth which changes sign between each vertical grid point.

Comparison of Fig. 3.1 and 3.2 shows that the vectors corresponding to the two different mean states are very similar with only minor differences in the details. The equivalent depths show greater differences where all but the external and first internal modes are about twice as large in the warm isothermal state. The external mode is about 25% greater and the first internal mode about 17%.

As was mentioned above, the vertical modes depend on the details of the vertical finite differencing. Table 3.2 also lists the equivalent depths for the 1 March 1965 case but with effective thickness of the top layer given by $(1/\sigma)_1 = (2\ell n(\sigma_{1\frac{1}{2}}/\sigma_1))/\sigma_{1\frac{1}{2}} = 78.5613$. Comparison of column (c) with (a) shows that this change primarily affects the first internal mode, reducing it a little more than 30%. The vectors are shown in Fig. 3.3. Comparison with Fig. 3.1 shows the major change is in the first internal mode which shows a relative decrease in its value at the top. The other modes show only minor changes.

b. Horizontal modes

As discussed in Section 2, the vectors $\underset{\sim}{Y}$ are the latitudinal normal modes, each longitudinal wavenumber k and equivalent depth D_m producing a different set. These latitudinal modes are traditionally divided into three groups - the slower westward propagating Rossby modes and the faster eastward and westward propagating gravity modes - according to their correspondence with the solutions of the continuous equations. Temperton (1977) points out that in this discrete system with finite depth the Rossby and gravity

modes are always clearly distinguishable in terms of their frequency.

The odd-indexed Rossby and even-indexed gravity modes are symmetric, i.e., u and h are symmetric about the equator and v is antisymmetric, while the even-indexed Rossby and odd-indexed gravity modes are antisymmetric. With the larger equivalent depths the number of zero crossings of each mode tends to increase with increasing index ℓ but the correspondence is not exact partly because of the finite equivalent depth and partly due to truncation error as the modes become very close to zero over certain latitude ranges. The magnitudes of the frequencies of the gravity modes increase with increasing index while those of the Rossby modes decrease. With small equivalent depths ($D \sim 1$ m) the horizontal modes do not seem to resemble the continuous modes, they tend to be more of a computational nature. Temperton (1977) provides more details and examples of the modes and compares them with the modes for second-order centered differences found by Dickinson and Williamson (1972).

4. Linear normal mode initialization

By definition, normal mode initialization, both linear and nonlinear, is a procedure which is applied in mode space and modifies the coefficients of selected normal modes in some prescribed way. Thus, given an initial grid point data field we must first expand into normal modes. The expansion is done sequentially following the analysis of Section 2. The mean state is first removed from the prognostic variables then the thermodynamic variables are combined by (2.22) to get the variable h used in the definition of the vertical modes. If the primary model thermodynamic variable is T rather than ϕ , ϕ must first be computed from (2.15) before obtaining h. The data are expanded into vertical modes using (2.32), and each vertical mode is expanded into Fourier modes using (2.41) then scaled according to (2.49). The symmetric and antisymmetric components are found by averaging or differencing the values from the two hemispheres. Finally, each scaled Fourier mode of each vertical mode is expanded into latitudinal modes by (2.56) or (2.57).

Once selected coefficients are modified, the expansion procedure is reversed to obtain grid point data. The scaled Fourier modes are obtained from (2.59) then unscaled by inverting (2.49). Vertical mode coefficients are obtained from the Fourier coefficients with (2.40) and symmetric and antisymmetric grid point data for u, v and h results from (2.37). The global grid point data are obtained from the sum of the symmetric and antisymmetric data for one hemisphere and from the difference for the other. However, given h we still must obtain p_s and ϕ or T by inverting (2.22) before adding the mean state back on.

In order to do the inversion we first obtain an expression for p_s in terms of h. Elimination of $\underset{\sim}{\delta}$ from (2.19) and (2.25) gives

$$\frac{\partial \ell n p_s}{\partial t} = g \underset{\sim}{\Pi}^T \underset{\sim}{C}^{-1} \frac{\partial \underset{\sim}{h}}{\partial t} + \left[Q p_s - g \underset{\sim}{\Pi}^T \underset{\sim}{C}^{-1} \underset{\sim}{Q}_h \right] \tag{4.1}$$

or for linear motions

$$\frac{\partial \ell n p_s}{\partial t} = g \underset{\sim}{\Pi}^T \underset{\sim}{C}^{-1} \frac{\partial \underset{\sim}{h}}{\partial t} \tag{4.2}$$

If the field consists of only one mode with frequency ν'_ℓ , (4.2) becomes

$$i\nu' \ell n p_s = i\nu'_\ell \, g \underset{\sim}{\Pi}^T \underset{\sim}{C}^{-1} \underset{\sim}{h} \tag{4.3}$$

which for nonzero ν'_ℓ gives

$$\ell n p_s = g \underset{\sim}{\Pi}^T \underset{\sim}{C}^{-1} \underset{\sim}{h} \tag{4.4}$$

Since (4.4) is linear in $\ell n\, p_s$ and $\underset{\sim}{h}$, it also holds for a sum of modes as long as each mode has a nonzero frequency.

The same expression (4.4) can be derived using the separation of variables approach of Williamson and Dickinson (1976) applied to the σ system equations. In this approach an assumed solution of the following form is substituted into the discrete equations.

$$
\begin{aligned}
u(\lambda_i,\theta_j,\sigma_n,t) &= u(\lambda_i,\theta_j,t)U_n \quad , \; n=1,\ldots,N \\
v(\lambda_i,\theta_j,\sigma_n,t) &= v(\lambda_i,\theta_j,t)U_n \quad , \; n=1,\ldots,N \\
T(\lambda_i,\theta_j,\sigma_n,t) &= Q(\lambda_i,\theta_j,t)T_n \quad , \; n=1,\ldots,N \\
\phi(\lambda_i,\theta_j,\sigma_n,t) &= Q(\lambda_i,\theta_j,t)\Phi_n \quad , \; n=\tfrac{1}{2},\ldots,N+\tfrac{1}{2} \\
\dot{\sigma}(\lambda_i,\theta_j,\sigma_n,t) &= \frac{\partial Q}{\partial t}(\lambda_i,\theta_j,t)S_n, \; n=\tfrac{1}{2},\ldots,N+\tfrac{1}{2} \\
\ell n p_s(\lambda_i,\theta_j,t) &= Q(\lambda_i,\theta_j,t)P
\end{aligned}
\tag{4.5}
$$

This separation of variables, which can only be done in the case of no mountains (ϕ_s = constant), is obtained by assuming that the continuity equation (2.7) can be written as two equations involving a separation parameter D. These equations become

$$(R\bar{T}_n P+\bar{\Phi}_n^{\sigma}) \frac{\partial Q}{\partial t} = - gDU_n \frac{1}{a\cos\theta}\left(\frac{\partial u}{\partial \lambda} + \frac{\partial v\cos\theta}{\partial \theta}\right) \tag{4.6}$$

$$P \frac{\partial Q}{\partial t} = \frac{1}{gD} \sum_{n=1}^{N} \frac{\partial Q}{\partial t}\left[R\bar{T}_n P+\bar{\Phi}_n^{\sigma}\right](\Delta\sigma)_n \tag{4.7}$$

and simplify to the following

$$\frac{\partial Q}{\partial t} = - gD \frac{1}{a\cos\theta}\left(\frac{\partial u}{\partial \lambda} + \frac{\partial v\cos\theta}{\partial \theta}\right) \tag{4.8}$$

$$(R\bar{T}_n P + \bar{\Phi}_n^{\sigma}) = U_n \tag{4.9}$$

$$P = \frac{1}{gD} \sum_{n=1}^{N} U_n(\Delta\sigma)_n \tag{4.10}$$

Equation (4.8) along with the results of substituting (4.5) into the momentum equations (2.1) and (2.2) give the shallow water equations for the horizontal structure $u(\lambda_i,\theta_j,t)$, $v(\lambda_i,\theta_j,t)$ and $Q(\lambda_i,\theta_j,t)$.

Equations (4.9) and (4.10) along with the results of substituting (4.5) into the hydrostatic (2.15) and thermodynamic (2.4) equations give the vertical structure equations. The vertical variables T_n, Φ_n, S_n and P can be eliminated from the vertical set to give an eigenvalue problem for gD with eigenvector U_n. The eigenvalue problem is the same as that of the matrix $\underset{\sim}{C}$ in (2.31), so the eigenvectors $\underset{\sim}{U}$ giving the vertical structure are the same as $\underset{\sim}{\Phi}$ of (2.28).

A complete solution of the grid point values is then a sum over all modes so that last equation of (4.5) for $\ell n\ p_s$ would actually be

$$\ell n p_s = \underset{\sim}{P}^T g \underset{\sim}{\bar{h}} \tag{4.11}$$

where $\underset{\sim}{P}^T$ has one component P from each vertical mode obtained from (4.10) and $\underset{\sim}{\bar{h}}$ is the vector of vertical mode coefficients of h (2.32). Equation (4.10) can be rewritten

$$\underset{\sim}{P}^T = \underset{\sim}{\Pi}^T \underset{\sim}{\phi} (g\underset{\sim}{D})^{-1} \tag{4.12}$$

Therefore,

$$\ell n p_s = \underset{\sim}{\Pi}^T \underset{\sim}{\phi} \underset{\sim}{\phi}^{-1} \underset{\sim}{C}^{-1} \underset{\sim}{\phi} g \underset{\sim}{\bar{h}} \tag{4.13}$$

or

$$\ell n p_s = \underset{\sim}{\Pi}^T \underset{\sim}{C}^{-1} g \underset{\sim}{h} \tag{4.14}$$

which is just the expression we had earlier (4.4). This equation states that, for linear modes, the surface pressure is determined uniquely from the h field which in turn is related to the linear horizontal velocity divergence. There is no reason to expect observed atmospheric data to satisfy (4.14) so that given h computed from observed data via (2.22), $\ell n p_s$ obtained from (4.14) will not necessarily agree with the original $\ell n p_s$. This is not surprising since the atmosphere

is not linear and the surface pressure reflects the non-linear mass divergence rather than the linear velocity divergence. Therefore it is not reasonable to use (4.4) or (4.14) to compute the surface pressure from the complete h field. It is, however, reasonable to use (4.4) or (4.14) to relate the changes made by the initialization procedure since to a large extent the procedure is subtracting out linear gravity waves.

Therefore, the change in surface pressure can be computed from

$$\Delta \ell n p_s = \underset{\sim}{\Pi}^T \underset{\sim}{C}^{-1} g \Delta \underset{\sim}{h} \tag{4.15}$$

where the Δ represents the change made by the initialization procedure,

$$\ell n p_s^* = \ell n p_s - \Delta \ell n p_s \tag{4.16}$$

$$h^* = \underset{\sim}{h} - \Delta \underset{\sim}{h} \tag{4.17}$$

and the asterisk indicates the initialized fields. The $\bar{\phi}^\sigma$ field is determined by inverting (2.22),

$$\bar{\underset{\sim}{\phi}}^{\sigma *} = g \underset{\sim}{h}^* - R \bar{\underset{\sim}{T}} \, \ell n p_s^* \tag{4.18}$$

and ϕ by inverting the $(^{-\sigma})$ operator integrating up from ϕ_s at the surface. One can just as easily compute the change in $\bar{\phi}^\sigma$ from

$$\Delta \bar{\underset{\sim}{\phi}}^{\sigma} = g \Delta \underset{\sim}{h} - R \bar{\underset{\sim}{T}} \, \Delta \ell n p_s \tag{4.19}$$

invert the $(^{-\sigma})$ operator integrating up from zero at the surface and subtract the change at the model grid points

$$\underset{\sim}{\phi}^{*} = \underset{\sim}{\phi} - \Delta\underset{\sim}{\phi} \tag{4.20}$$

These two procedures produce identical ϕ^{*} fields. If T is desired rather than ϕ, (2.20) and (2.22) can be combined and inverted to give

$$T^{*} = \underset{\sim}{G}^{-1}(g\underset{\sim}{h}^{*} - R\underset{\sim}{\bar{T}}\ell n p_{s}^{*} - \underset{\sim}{\phi}_{s}). \tag{4.21}$$

One can just as easily deal with changes in which case $\underset{\sim}{\phi}_{s}$ drops out of (4.21).

It was pointed out following (4.5) that the separation of variables approach of Williamson and Dickinson (1976) requires the assumption of no mountains (ϕ_{s}=constant). The approach of Section 2 does not seem to make that assumption, only that $\partial\phi_{s}/\partial t = 0$ in differentiating the hydrostatic equation (2.15) with respect to time. Yet the two approaches result in the same eigenvalue problems for the vertical and horizontal normal modes. Actually the analysis of Section 2 also assumes that the mean state is independent of time; for example, that the matrix $\mathscr{T}$ in (2.18) is independent of time. However, since the mean state is taken as a function of σ, this assumption is only valid if ϕ_{s} is a constant otherwise the mean state must change with time as determined from the governing equations. To solve the initial value problem for the perturbations (2.16)-(2.20) including mountains, the time evolution of the mean state must be included resulting in a problem with nonconstant coefficients which vary with time and space. This variation produces a nonseparable problem which is far too large to solve for operational model resolutions. Thus the approach of Section 2 does not determine the free oscillations of the model with mountains present and the modes found in Section 2 do not feel the mountains except possibly through

lower average temperature of the mean state if these temperatures are computed as observed averages on σ surfaces rather than p surfaces. Nevertheless the initialization procedure can be applied to a model with mountains. As we will see in the following section, there are problems in interpreting the linear modal initialization when mountains are included but these are corrected by the nonlinear initialization.

We are now in a position to consider how the mode coefficients are modified in the linear initialization. This procedure follows directly from examination of the equation for the time variation of the coefficients. For the linear case (2.58) becomes

$$\delta_t c(k,l,m) = - i\nu'(k,l,m)c(k,l,m) \qquad (4.22)$$

If the coefficients of unwanted gravity waves are set equal to zero initially, they will remain zero for ever in a linear model. This is essentially all that is done for linear normal mode initialization.

For a multi-level model, the question remains as to which of the model's gravity modes should be initialized in this linear procedure. We saw in Section 3 that the frequencies of the highest internal gravity modes (with the smallest equivalent depths) are so low that their presence in the initial data should be of no consequence. In practice, a convenient procedure is to zero all the gravity mode coefficients for the first m vertical modes.

In this section and those that follow, we describe initialization experiments using a 9-level, global model with a horizontal resolution of $\Delta\lambda=\Delta\theta = 3.75^{o}$. Largely on the basis of the experiments carried out by Andersen (1977), and our own preliminary experiments with the nonlinear initialization scheme described in Section 5, we chose m=5 for the linear

initialization experiment, i.e., all gravity mode coefficients were set to zero for the external and first four internal modes. Some justification for this choice was later provided by counting, for each vertical mode, the number of gravity modes with periods less than (a) 6 hours, (b) 12 hours. For the 3.75^{o} grid, the results are summarized in Table 4.1. There were no Rossby modes with periods less than 12 hours (this might not be the case if the basic state included a realistic zonal flow). Table 4.1 shows that eliminating the gravity modes for the first five vertical modes eliminates all gravity modes with periods less than 12 hours which seems a reasonable choice.

The initial data for our initialization experiments consisted of global fields of temperature, wind, and surface pressure for 00Z on 1 March 1965, as analysed at GFDL and subsequently interpolated to the ECMWF model's grid. The results of each initialization experiment were used as initial data for a 24-hour forecast, using explicit centered time differences with a time step of 300 seconds. At each time step, the values of selected variables at four horizontal grid points were written to a "grid point history file." The forecasts described here and in the following section were purely adiabatic, i.e., the "physics" parameterizations were excluded. Experiments which include such parameterizations are discussed in Sections 6 and 7. Time-filtering and horizontal diffusion were also switched off, in order to show up any high-frequency oscillations in the forecasts.

Fig. 4.1 shows the evolution of surface pressure at two horizontal grid points for two 24-hour forecasts, one from the original data, and one from the data modified by setting to zero the coefficients of the gravity modes for the first five vertical modes. (In all the figures of this type in this report, the values are plotted at every time step.) The forecast from the original data is severely contaminated by high-frequency oscillations, implying a poor state of

balance in the initial conditions. As in the shallow water experiments of Williamson (1976), linear normal mode initialization reduces the amplitude of the oscillations, but by no means eliminates them. In fact, comparison of Fig. 4.1 with Williamson's results suggests that linear normal mode initialization is rather less effective in a multi-level model with mountains than in a barotropic model without mountains.

Notice in particular the plots of surface pressure at 30 ^{o}N, 90 ^{o}E, a point over the Himalayas. Linear initialization has raised the surface pressure by ~ 12 mb compared with the original data, but as soon as the forecast starts the surface pressure falls by 15 mb in 2 hours.

Further evidence of the unsatisfactory performance of linear normal mode initialization in regions of high topography is presented in Fig. 4.2, which shows the geopotential height and wind fields at 500 mb and 1000 mb over Western Europe and the eastern Atlantic, before and after linear initialization. (Lowest model level winds are shown in the case of the 1000 mb map.) The initialization procedure has resulted in a sharp ridge over Greenland, where none existed before; in other regions of the chart the changes are relatively small. The spurious ridge is evident at 500 mb, and even more pronounced at 1000 mb. (Over Greenland the 1000 mb surface is fictitious, but examination of the surface pressures showed increases of up to 18 mb, accounting for the increase in the derived 1000 mb height.)

This behaviour is not difficult to explain. Over high topography there will be large deviations from the chosen basic state from which the normal modes are derived. As pointed out earlier, the derivation of the normal modes and thus the linear initialization procedure is in effect unaware of the presence of topography, and thus misinterprets

these large deviations as gravity waves, removal of which requires large adjustments to the mass field. Fortunately, as we shall see in the next section, this problem is solved by extending the normal mode initialization procedure to include nonlinear forcing.

5. Nonlinear normal mode initialization

We saw in the previous section that although the linear normal mode initialization reduces the gravity wave amplitudes in the forecasts, it does not eliminate them completely. The nonlinear terms of the model immediately regenerate the high frequency oscillations. Machenhauer (1977) proposed a nonlinear correction technique in which the coefficients of the undesired linear modes are not set to zero but rather to a value such that the time-tendencies of the undesired modes are zero initially.

The basis of Machenhauer's (1977) nonlinear correction to the normal mode initialization is the assumption that the nonlinear terms $r(k, \ell, m)$ in (2.58) have time variation much slower than the modes being modified and thus can be treated as constants. In this case the solution of (2.58) is

$$c(k,\ell,m,t) = \frac{r(k,\ell,m)}{i\nu'(k,\ell,m)} + \left[c(k,\ell,m,o) - \frac{r(k,\ell,m)}{i\nu'(k,\ell,m)}\right] e^{-i\nu t} \tag{5.1}$$

where for centered time differences the frequency ν is determined from

$$\nu' = + \frac{\sin \nu \Delta t}{\Delta t} \tag{5.2}$$

or for Crank-Nicholson implicit time differences from

$$\nu' = + \frac{\tan \nu \Delta t}{\Delta t} \tag{5.3}$$

With constant nonlinear terms $r(k,\ell,m)$, if the term in brackets in (5.1) is set to zero, the coefficients will be independent of time.

Since the nonlinear terms are not constant and in fact depend on the initial value of the mode coefficients, Machenhauer (1977) proposed to iterate in the following fashion to make the time change of the gravity wave coefficients zero,

$$\left[c(k,\ell,m,0)\right]_{\mu+1} = \frac{\left[r(k,\ell,m)\right]_{\mu}}{i\nu'(k,\ell,m)} \qquad (5.4)$$

where $\left[r(k,\ell,m)\right]_{\mu}$ is computed from the nonlinear terms using initial conditions from $\left[c(k,\ell,m,0)\right]_{\mu}$. Thus one can do a short forecast, say one time step, with the model, keep track of the nonlinear terms Q_u, Q_v, Q_T, Qp_s, then follow through the expansion procedure to get $r(k,\ell,m)$. However, it is easier to let the model automatically compile the nonlinear terms by computing the change in the coefficients over the short forecast and to then subtract off the linear part - the remainder being the transformation of the sum of all the nonlinear aspects of the model.

This approach is very convenient as it eliminates any need to modify the model code itself; however, one must be careful to analyse the actual time differencing used by the model. In the ECMWF model a forward time step is used initially. If $\delta_t c(k,\ell,m)$ in (2.58) is replaced by one forward time step, the nonlinear term is obtained from

$$r(k,\ell,m) = \delta_t c(k,\ell,m,0) + i\nu'(k,\ell,m)c(k,\ell,m,0) \; . \qquad (5.5)$$

The solution of (2.58) still has the form of (5.1) but the frequency is complex

$$\nu = \frac{\arctan\,(\nu'\Delta t)}{\Delta t} + \frac{i}{2\Delta t}\,\ell n\left[1 + (\nu'\Delta t)^2\right]$$

with an exponentially growing modification of the oscillatory part. This is just a restatement of the instability of forward differences but represents no problem when applied

to only the first time step. The condition to eliminate the damped oscillatory part of the coefficients is still that the term in brackets in (5.1) be zero. The iterative procedure (5.4) can be written

$$\left[c(k,\ell,m,0)\right]_{\mu+1} = \left[c(k,\ell,m,0)\right]_{\mu} + \frac{\left[c(k,\ell,m,\Delta t)\right]_{\mu} - \left[c(k,\ell,m,0)\right]_{\mu}}{i\nu'(k,\ell,m)\Delta t} \tag{5.6}$$

Note that although Δt appears explicitly in (5.6), the iterative procedure is independent of the choice of Δt as it actually cancels out in the forward difference.

To measure the convergence of the iterative procedure we use the sum of the squares of the time change of the coefficients as introduced by Andersen (1977)

$$BAL_m = \sum_{k=-K}^{K} \sum_{\ell \varepsilon G} \left[\delta_t c(k,\ell,m,0)\right] \left[\delta_t c(k,\ell,m,0)\right]^* \tag{5.7}$$

This balance is computed for each vertical mode, m, by summing over all longitudinal wavenumbers, k, and all latitude indices, ℓ, of the symmetric or antisymmetric gravity waves. The closer this measure is to zero for the gravity waves the closer the initial data are to the desired balance.

For comparison we also compute the balance (5.7) of the corresponding set of Rossby modes for which the inner sum is taken over all latitude indices of the symmetric or antisymmetric Rossby modes ($\ell \varepsilon R$) rather than gravity modes ($\ell \varepsilon G$). Of course, there is no reason for this balance to be zero. In the following we show these measures for the symmetric modes only, graphs of the antisymmetric modes are almost identical.

We first consider the number of vertical modes which need be included in the initialization procedure for the adiabatic 9 level, N24 model with mountains. In these experiments the nonlinear effects arise from the nonlinear advection or divergence terms in the basic dynamical equations without any forcing terms.

Fig. 5.1 shows the balance attained with four iterations of the nonlinear initialization (5.6) applied to the first 1, 2, 3, 4, 5, 7, and 9 vertical modes. Also shown for comparison is the balance of the Rossby waves, which is almost identical from one iteration to the next. Note that since the vertical modes are not orthogonal we cannot compare the amplitude of one vertical mode with that of another. The relative amplitudes of the various vertical modes depend only on the particular normalization used in defining these vectors and in our case have no physical meaning. The figure shows that the time change of the gravity waves of the original data (iteration 0) exceeds that of the Rossby modes for the first six vertical modes indicating a high degree of imbalance in this data set.

One iteration of (5.6) applied to all nine vertical modes reduces the time change in the gravity wave coefficients of all vertical modes except the last internal mode. It reduces the gravity wave time change to a level that is less than the Rossby wave change for all vertical modes except mode 3, the second internal mode. A second iteration results in an increase in the time change of all modes and with three iterations the procedure clearly diverges when all nine modes are included. This divergence of the higher internal modes is not surprising since the frequencies of the gravity waves corresponding to the small equivalent depths of Table 3.1 are very low and the fundamental assumption that the time scales of the nonlinear terms are much greater than those of the modes being modified is violated. The nonlinear interaction between

vertical modes probably then causes all the vertical modes to diverge.

Initialization of seven vertical modes also tends to show a divergence although much slower than with nine. The second iteration provides an improvement over the first in the first five modes with only a slight degradation of the sixth and seventh modes. The time change of the gravity waves for all vertical modes is less than that of the Rossby waves so this iteration might determine an adequate initial state. We will return to this possibility shortly when we examine the noise at individual grid points in the forecasts from these initial states.

The initialization procedure seems to converge when either the first five or four vertical modes are included, although not to zero values. The values after three and four iterations are very similar and not too different from those after two iterations. There is some indication that further iterations might diverge although we have not continued the procedure further. The procedure converges for the first three, two, or one vertical modes.

Although the iterative scheme does not converge to zero for the time change of the coefficients when five or more vertical modes are included, it may still be useful for practical applications. Two iterations with five vertical modes reduces the noise as measured by (5.7) in the external and first few internal modes by two to three orders of magnitude over the uninitialized data. In addition, there is no reason to reduce the noise to a level below a climatological level of the particular forecast model. Figures 5.2a and c show the plot of the surface pressure vs. time at a grid point over the central United States (40 ^{o}N, 90 ^{o}W) for forecasts from the uninitialized data and from data in which the first one to five vertical modes are initialized for two iterations. The uninitialized data produce a very noisy

forecast with oscillations of up to 8 mb and periods as small as 1/2 hour. Initialization of the external mode only reduces the amplitudes of the oscillations and eliminates the highest frequencies but considerable noise remains in the forecast. Inclusion of additional internal modes reduces the amplitudes of oscillation and eliminates the highest remaining frequencies so that with three modes initialized, the amplitudes are of the order of 1 mb and the shortest period a little less than eight hours. For all practical purposes initialization of five vertical modes eliminates all high frequency oscillations leaving just synoptic scale pressure variations.

Fig. 5.2b shows that high mountains do not adversely affect the initialization procedure. This figure shows the surface pressure at 30 ^{o}N, 90 ^{o}E over the Himalayas for forecasts from uninitialized data and data with the first three and five vertical modes initialized. The general characteristics of the curves are the same as over low smooth land (Fig. 5.2a).

Fig. 5.2d shows the difference between one and two iterations of five vertical modes for the point over the central U.S. (40 ^{o}N, 90 ^{o}W). Note that the two-iteration curve is the same as in Fig. 5.2a but with the scale greatly expanded. At this scale we see some high frequency oscillations in the forecast but their amplitudes are extremely small, being less than 0.1 mb. With one iteration only, the oscillations have amplitude of about 0.3 mb so that most of the improvement comes with the first iteration. The second does, however, provide additional improvement.

Fig. 5.3 shows a plot of $\dot{\sigma}$ vs. time at 40 ^{o}N, 90 ^{o}W and at 30 ^{o}N, 90 ^{o}E for forecasts from the uninitialized data and from data in which the first five vertical modes are

initialized for two iterations. As with the surface pressure, the noise present in the uninitialized case is eliminated by the procedure.

For each iteration of the initialization procedure, the next guess of the coefficients depends on the nonlinear terms (5.4) which include effects from all modes including the gravity waves. Therefore, it might make a difference whether or not the gravity waves of the initially unbalanced data are included in determining the nonlinear terms for the first iteration. To examine this possibility we made one run initializing the first five vertical modes. We first performed a linear initialization of these modes setting the coefficients of the gravity waves to zero followed by four nonlinear iterations. The balance attained at each iteration is shown in Fig. 5.4. The linearly initialized state shows some reduction in the noise when compared with the uninitialized data. The linear initialization reduces the noise by one order of magnitude in the external mode and half an order of magnitude in the first internal mode. The other internal modes are only slightly modified. This balance is not adequate for a smooth forecast as indicated earlier in Fig. 4.1. The balance after the additional non-linear iterations is just slightly lower than that starting from the uninitialized data although the difference may be insignificant in the forecast.

Although these two approaches, with or without a first linear initialization step, produce a similar balance after each nonlinear iteration, the question remains as to whether they result in the same initial state. Fig. 5.5 indicates that they do. This figure shows the 500 mb height contours and wind vectors for these two cases after two nonlinear iterations of the first five vertical modes over the same region as shown earlier in Fig. 4.2. for the linearly initialized data. The linear initialization resulted in great distortion in the height contours over

the mountains (Fig. 4.2) which succeeding nonlinear iterations remove (Fig. 5.5a). The two nonlinearly initialized cases, with and without a first linear step (Figs. 5.5a and b), result in practically the same state.

Fig. 5.6 shows a plot of surface pressure at 40 ^{o}N, 90 ^{o}W for a forecast starting from the data that were initialized linearly followed by two nonlinear iterations, all applied to the first five vertical modes. Comparison with the forecast from just two nonlinear iterations in Fig. 5.2a shows that the two forecasts are practically identical indicating that the first linear step has no influence and that the final balanced data depends only on the initial Rossby modes and not on the initial spurious gravity modes. The necessary balanced state is essentially determined by the nonlinear interactions between the Rossby modes.

Another question needing examination is the importance of using normal modes obtained from the actual mean temperature of the data being initialized. Fig. 5.6 shows the surface pressure at 40 ^{o}N, 90 ^{o}W during a forecast after two nonlinear iterations of the first five vertical modes using the normal modes for an isothermal 300 ^{o}K atmosphere. This can be compared with the corresponding curve in Fig. 5.2a which uses the modes for the actual mean temperature of the initial data. The 300 ^{o}K modes result in slightly larger oscillations, but the amplitudes are still less than a few tenths of a mb.

According to the measures examined here the nonlinear normal mode initialization works extremely well. It is also of interest for comparison to examine these same measures for other initialization schemes. We have only considered dynamic initialization which until now seemed to be the most promising approach for an operational forecasting environment. Temperton (1976) has shown that dynamic

initialization rapidly removes at least the external gravity mode from the initial conditions for a multilevel model forecast.

The balance measure (5.7) for the initial state determined from six hours of dynamic initialization using the scheme due to Okamura (Nitta, 1969) is shown in Fig. 5.7. This procedure principally reduces the noise in the external and first internal vertical modes with slight improvement in the second and third internal modes and very small change for the higher internal modes. The improvement is not anywhere near as great as that from just one iteration of the nonlinear modal initialization (Fig. 5.1) yet the dynamic initialization takes about 40 times as much computer time as one iteration of the nonlinear modal initialization. The surface pressure at 40 ^{o}N, 90 ^{o}W from the forecast from the dynamic initialization is shown in Fig. 5.6. This initialization eliminates the highest frequencies as expected but there still remain substantial oscillations with periods of eight hours which could be troublesome in a forecast.

The nonlinear normal mode initialization is shown above to be a very effective balancing procedure but does it result in a better forecast? The 500 mb and 1000 mb heights for 24 h forecasts from initialized and uninitialized data are shown in Fig. 5.8. Two nonlinear iterations, on the first five vertical modes, were performed for the initialization. North of 30^{o} the two forecasts are very similar, the major features are all centered at the same points and their amplitudes are very close. Equatorward of 30^{o} the forecasts are quite different. The uninitialized case shows the presence of gravity waves sloshing about with unrealistic height variations throughout the tropics.

Fig. 5.9 shows the global average height RMS and correlation coefficients of the two forecasts compared with the NMC analysis as a function of latitude and time. The initial-

ized forecast is clearly better than the uninitialized forecast in terms of the measures; however, the difference may be due to the gravity waves present in one and not the other. The Rossby-wave part of the solution may not be that different. To check this possibility the data of the forecast from the uninitialized case were also initialized before computing the skill score, i.e., two nonlinear iterations were carried out on the first five vertical modes after the forecast was made of the data at 0, 12, and 24 h. The skill scores of these two forecasts are then virtually identical so that it doesn't matter whether the balancing is done before or after the forecast but it does matter whether the balancing is done or not. The natural conclusion is that the high frequency gravity waves do not interact with the low frequency Rossby waves which is not surprising with a model that does not include forcing terms that might be influenced by the gravity waves. This might not be the case when the mode includes realistic physical processes such as release of latent heat which are strongly influenced by the vertical motion. In such models vertical motions associated with erroneous gravity waves could result in the release of latent heat which might force the solution to a different forecast. However, to observe such a result the model and initial moisture and vertical motions fields must be capable of producing condensation immediately in the forecast. The modal initialization provides initial vertical motions; however, the initial moisture distribution must also be consistent. Andersen (1977) reported no substantial differences in the 12 and 24 h precipitation with and without initialization in his experiments with the spectral model. However, Baede and Hansen (1977) show that the condensation required a two-day spin up in the forecast without initialization. This might be due to a deficient initial moisture field as well as a deficient initial vertical motion field in which case the initialization will not improve this aspect of the forecast.

6. Initialization with friction

One of the advantages of nonlinear normal mode initialization over other methods is that inclusion of non-adiabatic and irreversible processes ("physics") is, at least in principle, quite straightforward. In practice there are some problems. This section describes preliminary attempts to include a parameterization of boundary layer friction within the initialization procedure. This parameterization consists simply of a skin friction effect at the lowest model level, with no modelling of vertical momentum transfer between this level and the levels above. When included in a forecast, this parameterization generates very marked cross-isobar flow at the lowest model level.

We first examine the effect of running a forecast with friction from initial data produced by the adiabatic nonlinear initialization scheme described in Section 5 (2 iterations with 5 vertical modes included). Fig. 6.1 shows the plot of surface pressure during such a 24-hour forecast compared with that from a similar forecast starting from the original uninitialized data. The results are very similar to those from the corresponding forecasts without friction; the introduction of friction into the forecast does not significantly regenerate the gravity-mode oscillations removed by the adiabatic initialization. This implies that, in order simply to remove such oscillations from a forecast with a model including friction, it is not necessary to include friction in the initialization. On the other hand, for the initial data to be consistent both with the real atmosphere (as reflected in the analysis) and the model, it is clear that the effect of boundary layer friction should be incorporated. To measure the success of incorporating this effect, it is necessary to examine the initial state, rather than simply to check for the absence of spurious oscillations in the subsequent forecast.

Fig. 6.2a shows the 1000 mb geopotential height field and the lowest model level winds after 2 iterations of the non-linear initialization procedure, with 5 vertical modes initialized, and friction included in the nonlinear forcing. There is very little evidence of any cross-isobar flow. The initial state produced by the adiabatic initialization also lacks cross-isobar flow as does the uninitialized state. The reason for this lack even with friction included becomes clear on examining the structure of the vertical modes (Fig. 3.2); the frictional effect, which is non-zero only at the lowest model level, can only be resolved by including the very highest vertical modes, as the low order modes have no structure near the surface. The fact that these highest modes have very low frequencies also explains the absence of significant oscillation (Fig. 6.1).

We showed in Section 5 that the adiabatic initialization procedure diverges if all the vertical modes were included for more than one iteration, yet all vertical modes must be included to capture the effect of surface friction. Therefore, to include friction in the nonlinear forcing, we performed an experiment in which 5 vertical modes were initialized in the first iteration, and all 9 vertical modes in the second. Fig. 6.2b shows the resulting 1000 mb height field and lowest model level winds; the strong cross-isobar flow characteristic of this skin friction parameterization has been successfuly produced. Fig. 6.3 shows the plot of surface pressure during a 24-hour forecast with friction run from this initial data. This forecast runs successfully. However Fig. 6.4, which shows the "balance" (as defined in (5.7)) during the initialization, indicates that the procedure is dangerously close to instability, and indeed an experiment in which it was varied slightly by initializing 9 vertical modes in the first iteration and 5 in the second blew up altogether.

We have shown in this section that effects other than simple dynamics can be included within the nonlinear normal mode initialization procedure, but that caution is required. The experiments described here were rather unsatisfactory in that only a crude parameterization of surface friction was included. Also, the large charges forced in the highest vertical modes may lead to unrealistic vertical temperature profiles, and it is possible that the instability could be controlled by including a convective adjustment step after each iteration. This question will be examined in Section 7.

7. Initialization with physics

Following our nonlinear initialization experiments with an adiabatic version of the ECMWF model (Section 5) and with a version including friction (Section 6), we performed a series of experiments in which an attempt was made to incorporate a more complete "physics" package into the model used in the initialization procedure. The package included a convective scheme, nonlinear horizontal diffusion, turbulent vertical fluxes (including a boundary layer), precipitation and latent heat release (Tiedtke et al, 1979). Radiation was excluded, mainly for computational economy. For these experiments we used a 15-level, N48 ($\Delta\lambda = \Delta\theta = 1.875^{o}$) version of the ECMWF model. To check the results of the initialization, 24-hour forecasts were run using a semi-implicit leapfrog time integration scheme with a small time-filtering parameter ($\varepsilon = 0.05$).

A check was first made that the adiabatic nonlinear initialization scheme performed satisfactorily at this higher resolution. Again using data for 1st March 1965, Fig. 7.1a and b shows the "balance" as defined in Equation (5.7) for the symmetric gravity modes, with the first 5 or 10 vertical modes included in the procedure. In the 5-mode case, convergence was maintained for five iterations, with some indication of divergence setting in at the sixth iteration for the fifth vertical mode. In the 10-mode case, divergence begins to set in for the higher modes at the second iteration. No attempt was made to include all 15 modes (the highest of which has an equivalent depth of only 4 cm).

These experiments were then repeated with the physics package included in the nonlinear forcing. For the 5-mode case, Fig. 7.1c shows the resulting balance for the symmetric gravity modes; divergence is already setting in for the fifth vertical mode after two iterations, and all vertical modes are diverging by the third iteration. Fig. 7.2 shows

the 1000-mb height and the lowest model level winds after two iterations with the first five vertical modes, both with (b) and without (a) physics; there is virtually no difference between the two. As in the experiments of Section 6, the boundary layer forcing simply cannot be resolved by the first few vertical modes.

For the 10-mode case (not plotted), divergence was immediate and catastrophic with physics included. Various strategies were tried to prevent this divergence, including convectively adjusting the data before the initialization and/or after each iteration, and only initializing those gravity modes with a linear frequency higher than a specified cut-off value (rather than all horizontal gravity modes for a specified number of vertical modes). None of these devices was successful. We are forced to conclude, reluctantly, that the iteration procedure suggested by Machenhauer (1976) cannot be made to work for the higher internal vertical modes of a multi-level model, particularly with non-adiabatic terms included in the nonlinear forcing. This result might indeed have been expected, since Machenhauer's scheme depends on the assumption that the time-scale of the nonlinear forcing is long compared with that of the modes being initialized; and it would not be surprising if this assumption were violated for the higher vertical modes in the presence of forcing by physical parameterizations.

Fortunately, it appears that in order to eliminate high-frequency gravity-mode oscillations from a forecast with a model which includes the physics package, adiabatic non-linear initialization is quite adequate. Fig. 7.3 shows the plot of surface pressure at 40 ^{o}N 90 ^{o}W during three 24-hour forecasts with the 15-level high-resolution model including physics. The solid line shows the evolution

during the forecast from the original data; as in the 9-level lower-resolution adiabatic case there are large oscillations. The dash-dot line shows the evolution in the corresponding forecast after two iterations of adiabatic nonlinear normal mode initialization, with the first five vertical modes included. Although the improvement is not quite as dramatic as in the 9-level adiabatic forecast, the initialization scheme can still be rated as very successful in terms of reduction of high-frequency noise. Further improvement was in fact obtained by applying two more iterations of the normal mode procedure, dashed line in Fig. 7.3.

Neither the original data nor the initialized data (as shown in Fig. 7.2) reflected the effect of friction in the boundary layer. As mentioned previously, this effect can only be resolved by including the higher internal vertical modes - which cannot be included in the initialization scheme. However, by a similar argument, if the boundary layer effects are present in the original data, they will not be removed during an adiabtic initialization involving only the first few vertical modes. To demonstrate this, the fields from the 24-hour forecast with physics (from the original uninitialized data) were saved and then subjected to two iterations of adiabatic initialization with five vertical modes included. Fig. 7.4 (a) shows the 1000 mb height and lowest model level winds from the 24-hour forecast; the effect of the boundary-layer parameterization can be seen in the cross-isobar flow, especially over land. Fig. 7.4 (b) shows the corresponding fields after initialization. Slight changes can be seen in the fields, but the cross-isobar flow has been retained.

Thus, in the context of an analysis/initialization/forecast cycle, provided that the effect of friction is reflected in the analysis near the surface (with the help of first-

guess fields from the forecast model including the physics package), this effect will not be destroyed by the initialization step. The same is presumably also true of any other physical effects which can only be resolved by the higher internal vertical modes of the model.

8. Interaction with analysis

Although the nonlinear modal initialization does not affect the forecast of the Rossby waves in the adiabatic model as indicated at the end of Section 5, it may be very useful in an operational forecast-analysis cycle. The presence of large amplitude gravity waves in a short forecast which is used as a background field by an analysis scheme will surely affect the resulting analysis in data poor regions and possibly in data-rich areas. In fact, in a preliminary 6 h forecast-analysis cycle carried out at ECMWF starting from the DST analysis of Lorenc et al (1977), the gravity wave noise caused considerable problems with the data checking routines. Because observations differed too much from the background field, they tended to be rejected whereas it was actually the noisy background field which was unrealistic. This problem arose in preparation for the analysis after the first 6 h forecast and the cycle was stopped. When the non-linear modal initialization was included in the cycle, no similar problems were noticed.

The problem may have arisen because the forecast started from an analysis which used a climatological first guess and which would therefore be more unrepresentative of or inconsistent with the actual state over data poor regions than if a forecast had been used. After a few cycles of the analysis-forecast procedure, the initialization might be unnecessary as the model propagates information into the data void regions and the global analysis becomes more consistent. To determine whether this is the case we examined the balance (5.7) of the analyses after several 6 h analysis-initialization-forecast cycles. Fig. 8.1 gives the time change of the coefficients of the gravity modes and Rossby modes in the analyses at 0, 6, 12, and 66 h. Time 0 is the analysis based on a climatological first guess, all the others are based on a 6 h forecast first guess from the preceding analysis. The noise in the gravity waves is greatest at time 0 but is not

insignificant in the later analyses. It is only reduced by half an order of magnitude in any of the analyses using a forecast first guess, even after 11 cycles. This measure is still at a high enough level for all the analyses to indicate that the forecast will have considerable noise if the initialization were omitted. Therefore, the nonlinear modal initialization is a useful part of the forecast-analysis cycle even after many cycles, not just for the first cycle.

It is also informative to examine the size of the change made by the initialization. The global RMS difference between the analysis and initialized data computed on σ surfaces is plotted in Fig. 8.2 for surface pressure, ϕ_6, V_6 and V_8. The differences are two to three times larger with the first analysis based on a climatological first guess than with any of the succeeding analysis based on a forecast first guess. The differences are nearly the same for all these succeeding analyses with the surface pressure difference slightly less than 1 mb, the vector wind at the eighth level less than 1.5 m s^{-1} and the geopotential and wind at the sixth level less than 25 m and 1 m s^{-1}, respectively. These average differences are within the average observational errors.

Although the average change made by the initialization is within observational errors, the changes at individual grid points might be relatively large even over northern hemisphere land areas with adequate observations. Daley (1978) proposed coupling the normal mode initialization with a variational approach wherein a weighted sum of the changes at grid points is minimized while the nonlinear initialization (5.4) served as a strong constraint. The weights could be proportional to the expected error of the original analysis. Such a procedure results in a complicated nonseparable variational problem which can only be solved practically by iterative procedures.

Daley (1978) tested it with a barotropic model successfully. Nevertheless, it is worthwhile to determine if a simpler procedure might serve the same purpose.

Machenhauer (1977) tested a procedure similar in concept to the insertion of data in four-dimensional assimilation but the adjustment is performed by the nonlinear initialization rather than by a model forecast and only data at one time are involved. After the nonlinear initialization, the "correct" data are restored, i.e., the initialized values are replaced by the observed values. These hybrid data are then reinitialized, "correct" data restored again and the process is repeated until some sort of convergence is attained, the convergence can be measured by the difference between the "correct" data and the initialized data. Machenhauer (1977) performed two tests with the shallow water equations; one in which the height field was assumed to be correct everywhere and the other in which the stream function field was assumed correct everywhere. The procedure did converge in both cases, the case of restoring the height field rather slowly and that of restoring the stream function field rather rapidly.

These two cases are extremely idealized; we never have a correct height field everywhere nor a correct wind field everywhere. Instead, analyses produce estimates of the height and wind fields everywhere with varying degrees of fidelity. One advantage of the optimum interpolation analysis method designed for the ECMWF operational suite (Lorenc et al, 1977) is that, as a byproduct, it produces estimates of the local error in the analyses. This error information could be used so that an initialization procedure makes the largest changes where the analysis is least reliable.

We have performed one preliminary experiment which modifies Machenhauer's (1977) approach to use this information. Essentially after each initialization in the insertion-initialization cycle, if the changes made by the initialization exceed one standard deviation of the expected analysis error at any grid points, the changes are reduced to be one standard deviation at these points. To avoid discontinuities, the changes at all grid points are actually given by the B^n function

$$B^n(\delta) = \left[\tanh(\delta^n)\right]^{\frac{1}{n}} \qquad (8.1)$$

where δ is the change made by the initialization procedure at a grid point measured in units of error standard deviations at that point and $B^n(\delta)$ is the change actually inserted before the next initialization. The B^n function shown in Fig. 8.3 for various values of n has the property that as n becomes large $B^n(\delta)$ equals δ for $\delta<1$ and equals 1 for $\delta>1$. For small n it provides a smooth transition between the linear and constant regions. For our experiment we choose n=2. The initialization consists of two iterations with the first five vertical modes with the adiabatic model.

We performed this procedure for three cycles using the analysis and analysis errors for the DST case analysed by Lorenc et al (1977). Table 8.1 shows the number of points exceeding one standard deviation for a few selected variables after the initialization of each cycle. We see that surface pressure and geopotential in the upper regions of the model are being forced closer by this measure to the analysis while the winds are straying away from the analysis. This probably is a result of the fact that the winds have many more points with changes less than one standard deviation than surface pressure and upper level geopotential and the procedure is proportioning the change more evenly. The lowest level geopotentials don't have large changes since they are determined to a larger extent by the surface geopotential.

Fig. 8.4 indicates that the procedure is converging. The lower curves show the RMS difference between the current and previous initialized field. After three cycles this difference is less than 0.2 mb for suface pressure and $0.22\,m\ s^{-1}$ for the vector wind at level 6. The upper curves show the RMS differences between the fields after the values are set to be less than one standard deviation and the following initialization, i.e., the change made by the initialization. At cycle 0 this is the difference created by initializing the original analysis. The changes made by the initialization are greatly reduced with just a few cycles.

The above experiment indicates that the procedure may work in an operational environment. However, it seems premature at this time to refine such a procedure until both the model and analysis scheme are more firmly fixed in their final operational forms and we have more reliable first-guess and observational error estimates as input for the analysis scheme.

9. DISCUSSION

9.1. Changes in finite-difference scheme

The initialization scheme described in this report is based on the normal modes of the finite-difference model linearized about a particular basic state. For simplicity we chose a basic state at rest, following the demonstration by Machenhauer (1977) that no significant improvement resulted from choosing for example a basic state with zonal flow. Similarly, we have shown in Section 5 that the choice of basic vertical temperature structure is not critical. In general, we can say that changes in the basic state are simply compensated by changes in the nonlinear forcing; and the splitting of the time derivatives of the model variables into linear and nonlinear contributions is to some extent arbitrary.

By the same token, minor changes in the model's finite-difference scheme do not necessarily require corresponding changes in the normal modes used for initialization. During the course of our experiments, a change was made to the form of the Jacobian term in the ECMWF gridpoint model (both are described in Burridge and Haseler, 1977). Linearizing the new Jacobian gives a different form of the Coriolis term in Equations (2.42) and (2.43), with the inconvenient result that the matrix L in Equation (2.51) is no longer symmetric (reflecting the fact that the new finite-difference scheme is no longer energy-conserving).

However, because of the approach described in Section 5, in which the forecast model automatically compiles the nonlinear terms, no change is required to the initialization procedure. The small difference between the linearized forms of the new Jacobian and the old is automatically absorbed into the nonlinear forcing. Fig. 9.1 shows the plot of surface pressure during an adiabatic 24-hour forecast, before and after nonlinear initialization (2 iterations,

5 vertical modes); in both cases the model used in the initialization and forecast included the new Jacobian term, but the normal modes used for initialization were based on the old. Comparison with Fig. 5.2 shows no deterioration in the results.

9.2 Changes in model grid

The computational feasibility of normal mode initialization depends crucially on the fact that the model's linearized equations are separable in the vertical and horizontal directions. Application to global (or hemispheric) grid-point models based on anything other than a regular latitude-longitude grid seems to be ruled out.

Limited-area models based on a regular latitude-longitude grid can probably be handled; the corresponding normal modes should be derived under the assumption that the time-derivatives are zero at any non-periodic boundaries (unless these are regarded as free-slip walls), and non-homogeneous boundary conditions could be absorbed into the nonlinear forcing. Limited-area models based on stereographic projections may possibly be amenable to nonlinear normal mode initialization provided that the domain is rectangular--any other shape would not allow the required separability. It would presumably be necessary to set up the linearized equations assuming a constant Coriolis parameter and constant map factors (or at least a function of one coordinate only), and to absorb deviations from these constant values into the "nonlinear" terms; for this reason the procedure is likely to work only for limited-area models of modest horizontal extent. Further study is required before a firmer assessment can be made of the applicability of normal mode initialization to limited-area models.

9.3 High-resolution models

One computational aspect of normal mode initialization which has not yet been mentioned concerns the determination and storage of the horizontal normal modes. Having separated the linear problem vertically, longitudinally, and into symmetric/antisymmetric modes, we obtain a large number of sizeable matrices whose eigensystems must be computed. This can of course be done once and for all as long as the results can be stored. For a model with L levels and M gridpoints between pole and equator, the storage required (assuming $\Delta\lambda = \Delta\theta$) amounts to approximately $36 \times L \times M^3$ words. Examples for several grid resolutions are given in Table 9.1, from which it is clear that a severe storage problem exists for global high-resolution models.

This difficulty can to some extent be alleviated by modifying the computational procedure outlined in Section 5, in such a way that the only eigenvectors which need be stored are those corresponding to normal modes which are modified by the nonlinear initialization scheme, i.e. only the gravity mode vectors for a certain number of vertical modes or whose frequencies are greater than some specified cut-off value.

Equation (5.6) can be written in the form

$$\Delta c(k,\ell,m,0) = \frac{\left[\delta_t c(k,\ell,m,0)\right]_\mu}{i\nu'(k,\ell,m)} \qquad (9.1)$$

where Δc is the change in a normal mode coefficient from one iteration of the nonlinear initialization scheme to the next. The time increment $\delta_t c$ was determined in Section 5 by expanding gridpoint fields at $t = o$ and $t = \Delta t$ in terms of normal mode coefficients, and taking the difference of the two resulting coefficient fields. However, since the transformation from gridpoint to normal mode space consists of a sequence of linear operations and the time

difference is linear, we can equally well perform the transformation directly on the time-derivatives of the gridpoint fields. (These can be obtained either by differencing the gridpoint fields from the forecast model at $t = 0$ and at $t = \Delta t$, or by writing a special version of the model which writes out a field of time derivatives instead of a "forecast" field at $t = \Delta t$). Similarly, rather than using Equation (5.6) to determine new values of $c(k,\ell,m,0)$ and then performing an inverse transformation to give a new field of gridpoint values, we can instead use Equation (9.1) to determine values of $\Delta c(k,\ell,m,0)$ and then transform this set of increments back to gridpoint space, where they can be added on the old gridpoint fields. The device used in Section 4 to separate changes in the pseudo-height variable h into changes in p_s and T fits conveniently into this modified procedure.

It is easy to see that the transformation between gridpoint and normal mode space required in this alternative procedure involves only the eigenvectors corresponding to normal modes which are to be modified. Thus the storage required to initialize the first five vertical modes of a model with $M = 48$ and any number of levels is reduced to $\sim 14 \times 10^6$ words. Experiments with such a model (with 15 levels) have been performed on the Cray-1 at ECMWF; storage requirements were in fact further reduced by "packing" the eigenvectors four to a 64-bit word. By scaling the eigenvectors and storing them as 16-bit integers this allowed sufficient accuracy, while reducing the storage to 3.5×10^6 words--about twice the size of a gridpoint data set at this resolution. The modified procedure has the additional advantage that it becomes unnecessary to save a file of normal mode coefficients from one iteration to the next.

It is worth mentioning that this storage problem is peculiar to gridpoint models, since they require considerably more degrees of freedom than spectral models for comparable accuracy. From figures given by Andersen (1977) it appears that storage requirements for the normal modes of spectral models will be quite modest for any likely resolution.

9.4 Initial conditions for semi-implicit forecasts

In comparison with explicit schemes, the semi-implicit time integration scheme achieves its computational economy at the expense of reduced accuracy in the treatment of gravity waves. Janjic and Wiin-Nielsen (1977) have argued that this may lead to misrepresentation of the geostrophic adjustment mechanism and consequently less accurate forecasts of the Rossby modes in semi-implicit integrations run from unbalanced initial data. However, experiments at ECMWF have shown that differences between explicit and semi-implicit forecasts become negligible when normal mode initialization has been applied to the initial fields before the forecasts.

9.5 Diagnostic applications

Besides providing improved initial conditions for numerical forecasts, normal mode initialization may be a useful technique in diagnostic studies. For example, the determination of certain energy budget statistics from analysed data requires the specification of a field of vertical motion. The results may be quite sensitive to the way in which this is done, and the application of nonlinear normal mode initialization may well be the best available means of specifying a vertical velocity field, although the fidelity of such a vertical motion field still depends on the quality of the model used to specify the nonlinear terms.

References

Andersen, J.H. 1977 A routine for normal mode initialization with non-linear correction for a multi-level spectral model with triangular truncation. ECMWF Internal Report No.15, 41 pp.

Baede, A.P.M. and Hansen, A.W. 1977 A ten-day high-resolution non-adiabatic spectral integration; a comparative study. ECMWF Technical Report No.7, 81 pp.

Baer, F. 1977 Adjustment of initial conditions required to suppress gravity oscillations in nonlinear flows. Contrib. Atmos. Phys., 50, 350-366.

Baer, F. and Tribbia, J. 1977 On complete filtering of gravity modes through non-linear initialization. Mon. Wea. Rev., 105, 1536-1539.

Bengtsson, L. 1975 Four-dimensional assimilation of meteorological observations. GARP Publication Series NO.15,76 pp.

Benwell,G.R.R.and Bretherton, F.P. 1968 A pressure oscillation in a 10-level atmospheric model. Q.J.Roy.Met.Soc., 94, 123-131.

Bourke, W. 1974 A multi-level spectral model. I. Formulation and hemispheric integrations. Mon.Wea.Rev., 102, 687-701.

Burridge, D.M. and Haseler, J. 1977 A model for medium range weather forecasting - adiabatic formulation. ECMWF Technical Report No.4, 45 pp.

Daley, R. 1978 Variational non-linear normal mode initialization. Tellus, 30, 201-218.

Daley, R. 1979 The application of non-linear normal mode initialization to an operational forecast model. Atmosphere-Ocean (in press).

Dickinson, R.E. and Williamson, D.L. 1972 Free oscillations of a discrete stratified fluid with application to numerical weather prediction. J.Atmos.Sci., 29, 623-640.

Flattery, T.W.	1970	Spectral models for global analysis and forecasting. Proc.Sixth AWS Technical Exchange Conf., U.S.Naval Academy, Air Weather Service Technical Report 242, pp.42-53.
Hoskins, B.J. and Simmons, A.J.	1975	A multi-layer spectral model and the semi-implicit method. Q.J.Roy.Met.Soc., 101, 637-655.
Houghton, D. and Washington, W.	1969	On the global initialization of the primitive equations: Part I. J.Appl.Met., 8, 726-737.
Houghton, D. Baumhefer, D.P. and Washington, W.M.	1971	On global initialization of the primitive equations: Part II, The divergent component of the horizontal wind. J.Appl.Met., 10, 626-634.
Janjic, Z. and Wiin-Nielsen, A.	1977	On geostrophic adjustment and numerical procedures in a rotating fluid. J.Atmos.Sci., 34, 297-310.
Lorenc, A. Rutherford, I. and Larsen, G.	1977	The ECMWF analysis and data-assimilation scheme: Analysis of mass and wind fields. ECMWF Technical Report No.6, 46 pp.
Machenhauer, B.	1977	On the dynamics of gravity oscillations in a shallow water model, with application to normal mode initialization. Contrib.Atmos.Phys., 50, 253-271.
Miyakoda, K. and Moyer, R.W.	1968	A method of initialization for dynamical weather forecasting. Tellus, 20, 115-128
Nitta, T.	1969	Initialization and analysis for the primitive equation model. Proc. of the WMO/IUGG Symposium on Numerical Weather Prediction, Tokyo, Japan, 26 Nov-4 Dec 1968, pp. VI, 11-20 Japan Meteorological Agency, Tokyo, 1969.
Nitta, T. and Hovermale, J.B.	1969	A technique of objective analysis and initialization for the primitive forecast equations. Mon.Wea.Rev., 97, 652-658.

Phillips, N.A.	1960	On the problem of initial data for the primitive equations. Tellus, 12, 121-126
Stephens, J.J.	1970	Variational initialization with the balance equation. J.Appl.Met., 9, 732-739.
Temperton, C.	1976	Dynamic initialization for barotropic and multilevel models. Q.J.Roy.Met.Soc., 102, 297-311.
Temperton, C.	1977	Normal modes of a barotropic version of the ECMWF grid point model. ECMWF Internal Report No.12, 38 pp.
Tiedtke, M. Geleyn, J.-F. Hollingsworth, A. and Louis, J.-F.	1979	ECMWF model-parameterization of sub-grid scale processes. ECMWF Technical Report No.10, 46 pp.
Williamson, D.L.	1976	Normal mode initialization procedure applied to forecasts with the global shallow water equations. Mon.Wea.Rev., 104, 195-206.
Williamson, D.L. and Dickinson, R.E.	1976	Free oscillations of the NCAR global circulation model. Mon.Wea.Rev., 104, 1372-1391.

Table 3.1 σ levels of model

vertical grid index	σ
$\frac{1}{2}$	0.00000
$1\frac{1}{2}$	0.03429
$2\frac{1}{2}$	0.12620
$3\frac{1}{2}$	0.25926
$4\frac{1}{2}$	0.41701
$5\frac{1}{2}$	0.58299
$6\frac{1}{2}$	0.74074
$7\frac{1}{2}$	0.87380
$8\frac{1}{2}$	0.96571
$9\frac{1}{2}$	1.00000

Table 3.2 Equivalent depths (m) and corresponding phase speeds (m s^{-1}) of gravity waves on nonrotating earth for mean state given by (a) average of 1 March 1965, (b) 300 ^{o}K, and (c) average of 1 March 1965 but with modified $(1/\sigma)_1$

	vertical mode index	(a)	(b)	(c)
depth (D)	1	11,502.5	14,664.8	10,153.1
	2	7,014.8	8,255.4	4,701.0
	3	960.85	1,798.7	851.40
	4	209.69	494.5	205.05
	5	65.43	157.9	64.90
	6	20.12	53.74	20.06
	7	7.287	17.66	7.275
	8	2.357	4.866	2.366
	9	.498	.809	.498
phase speeds ($\sqrt{gD}$)	1	335.74	379.10	315.44
	2	262.19	284.43	214.64
	3	97.04	132.77	91.34
	4	45.33	69.61	44.83
	5	25.32	39.34	25.22
	6	14.04	22.95	14.02
	7	8.45	13.16	8.44
	8	4.84	6.91	4.82
	9	2.21	2.82	2.21

Table 3.3 $\bar{T}(\sigma)$ for 1 March 1965

vertical grid index	$\bar{T}(\sigma)$
1	229.304
2	209.450
3	218.147
4	237.600
5	256.647
6	268.710
7	277.454
8	283.131
9	285.666

Table 4.1 Number of gravity modes (out of a maximum possible 4806) with periods less than (a) 6 hours, (b) 12 hours

vertical mode	(a)	(b)
1	4578	4602
2	4554	4598
3	4218	4539
4	1979	2622
5	0	40
6-9	0	0

Table 8.1 Number of points with differences greater than one standard deviation of expected analysis error

iteration	ϕ_3	ϕ_6	ϕ_9	u_6	u_9	v_6	v_9	p_s
1	2222	3950	4454	3770	3276	4169	3570	1556
2	2677	3733	4452	3627	3247	3946	3513	1894
3	2900	3674	4448	3491	3148	3808	3433	2112

Table 9.1 Storage requirements for normal modes

L = no. of levels; M = $\pi/2\Delta\theta$	Words
L = 9, M = 24 (model used in this report)	4.5×10^6
L = 15, M = 48 (possible operational model)	60×10^6
L = 15, M = 60 (possible operational model)	117×10^6

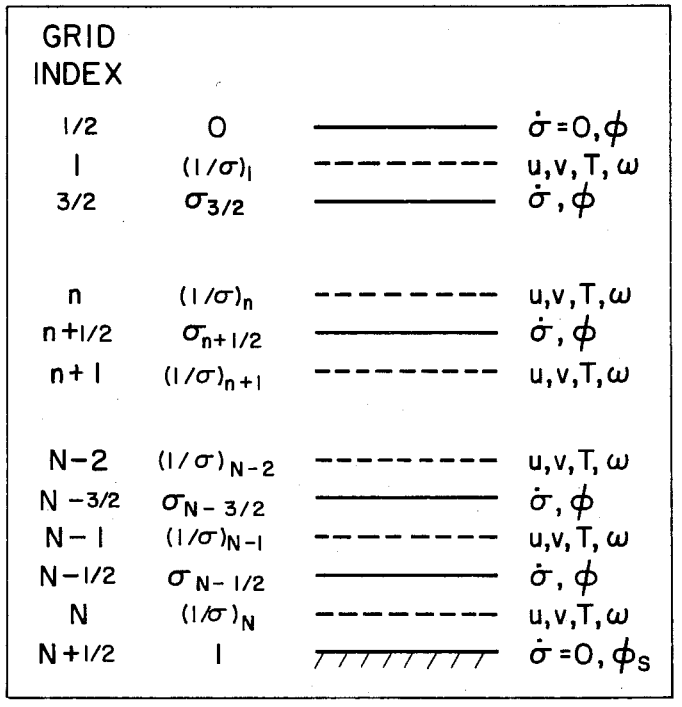

Fig. 2.1 ECMWF grid point model vertical grid.

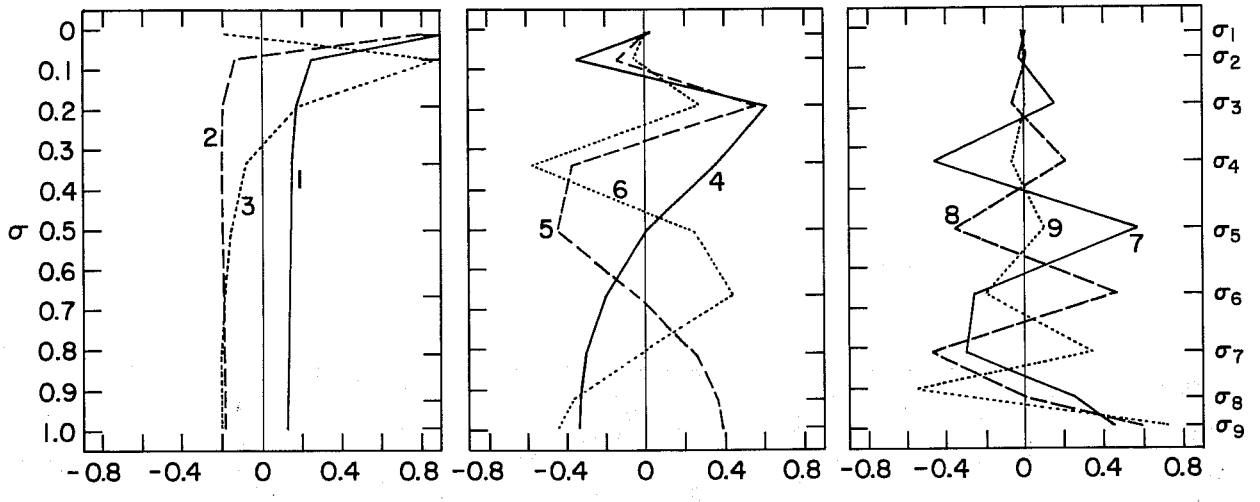

Fig. 3.1 Vertical modes with $\overline{T}(\sigma)$ from average of 1 March 1965.

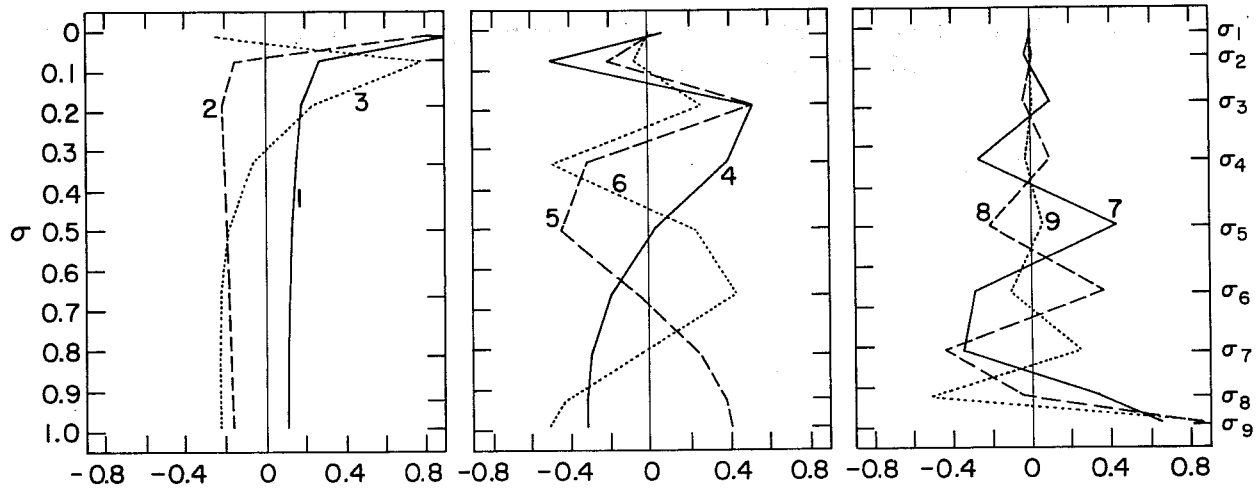

Fig. 3.2 Vertical modes with isothermal $\overline{T}(\sigma)$ = 300K.

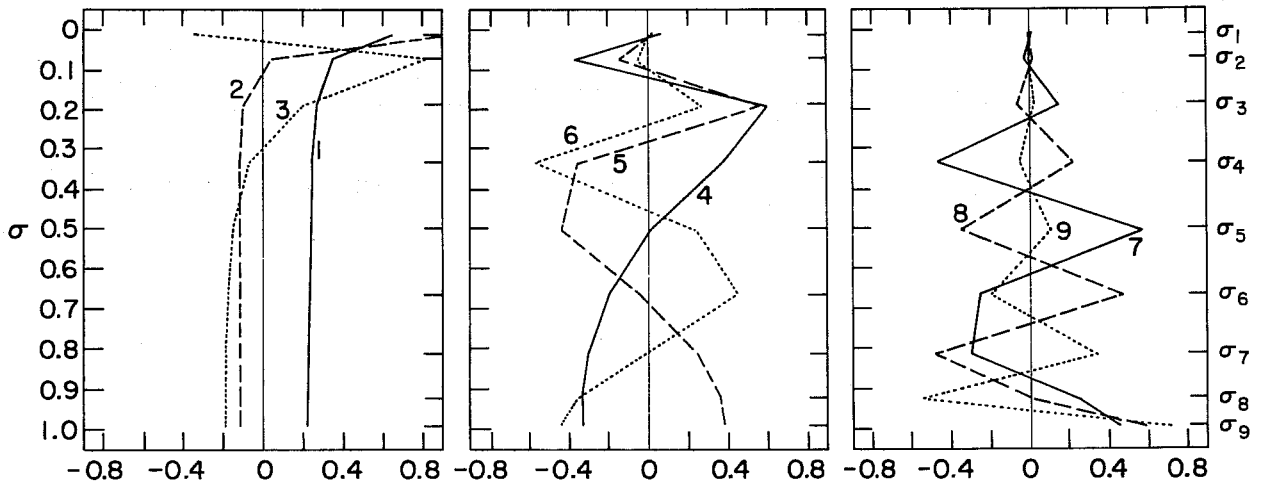

Fig. 3.3 Vertical modes with $\overline{T}(\sigma)$ from average of 1 March 1965 with modified $(1/\sigma)_1$.

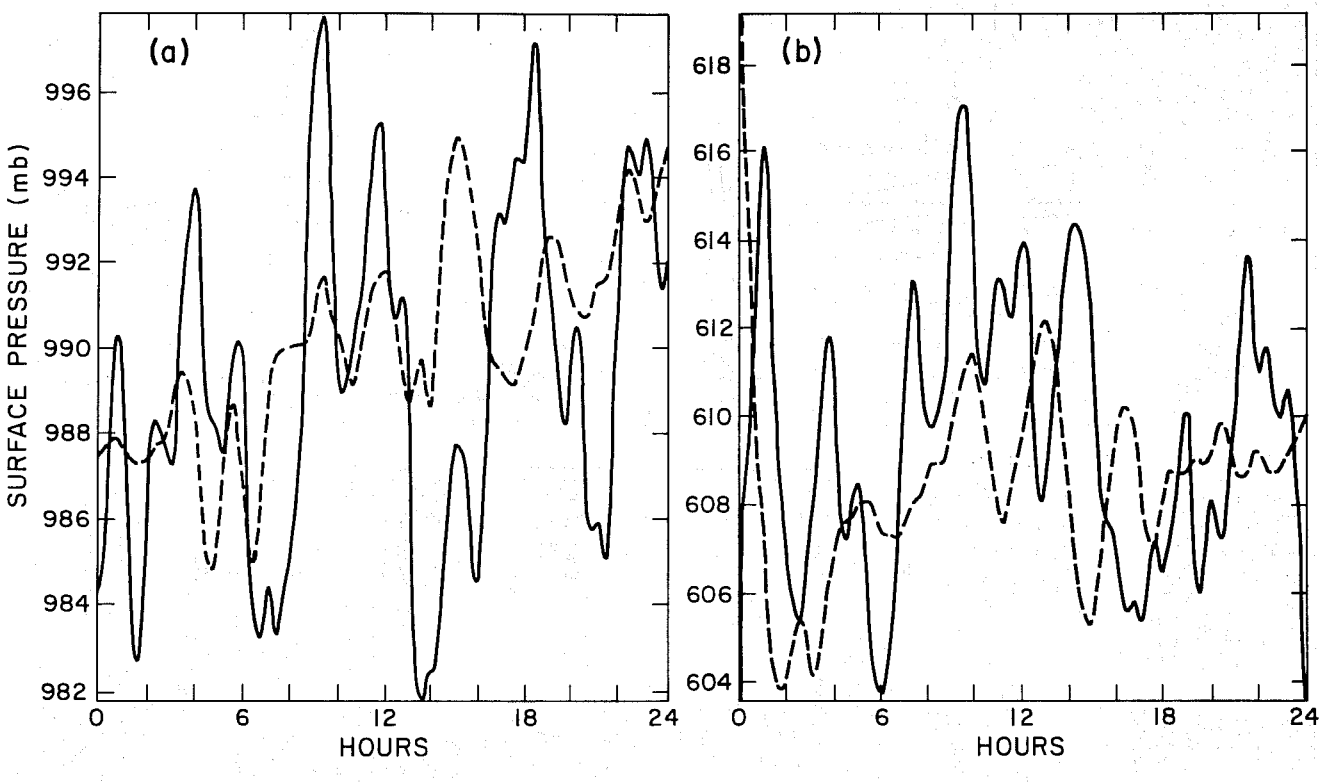

Fig. 4.1 Surface pressure vs time before (solid line) and after (dashed line) linear normal mode initialization: (a) at 40 ^{o}N, 90 ^{o}W; (b) at 30 ^{o}N, 90 ^{o}E.

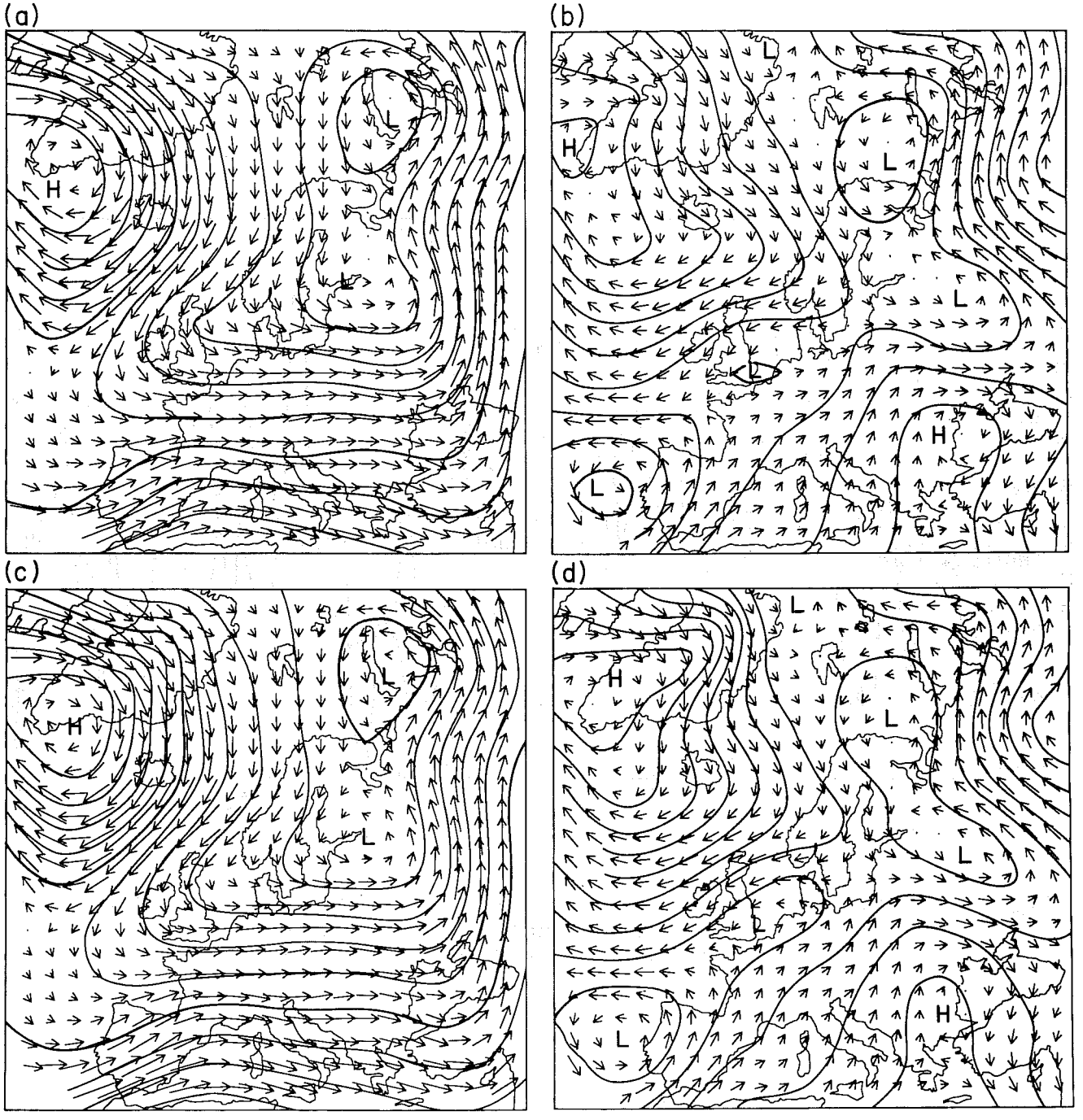

Fig. 4.2 (a) 500 mb geopotential height and wind fields, original data,
(b) 1000 mb geopotential height and wind fields, original data,
(c) 500 mb geopotential height and wind fields after linear normal mode initialization, and
(d) 1000 mb geopotential height and wind fields after linear normal mode initialization.

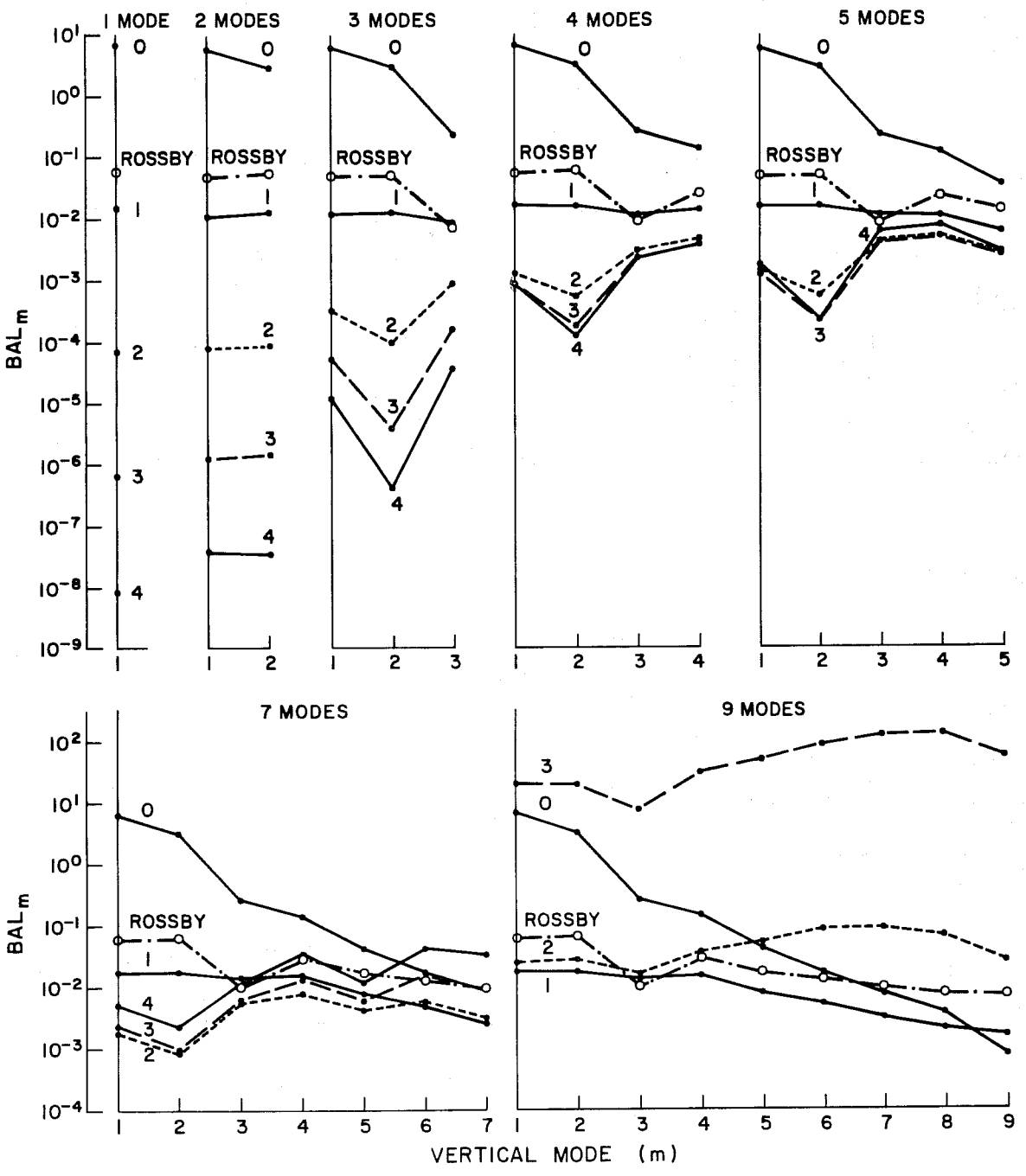

Fig. 5.1 Balance as measured by (5.7) of the symmetric gravity modes after n nonlinear iterations of m vertical modes.

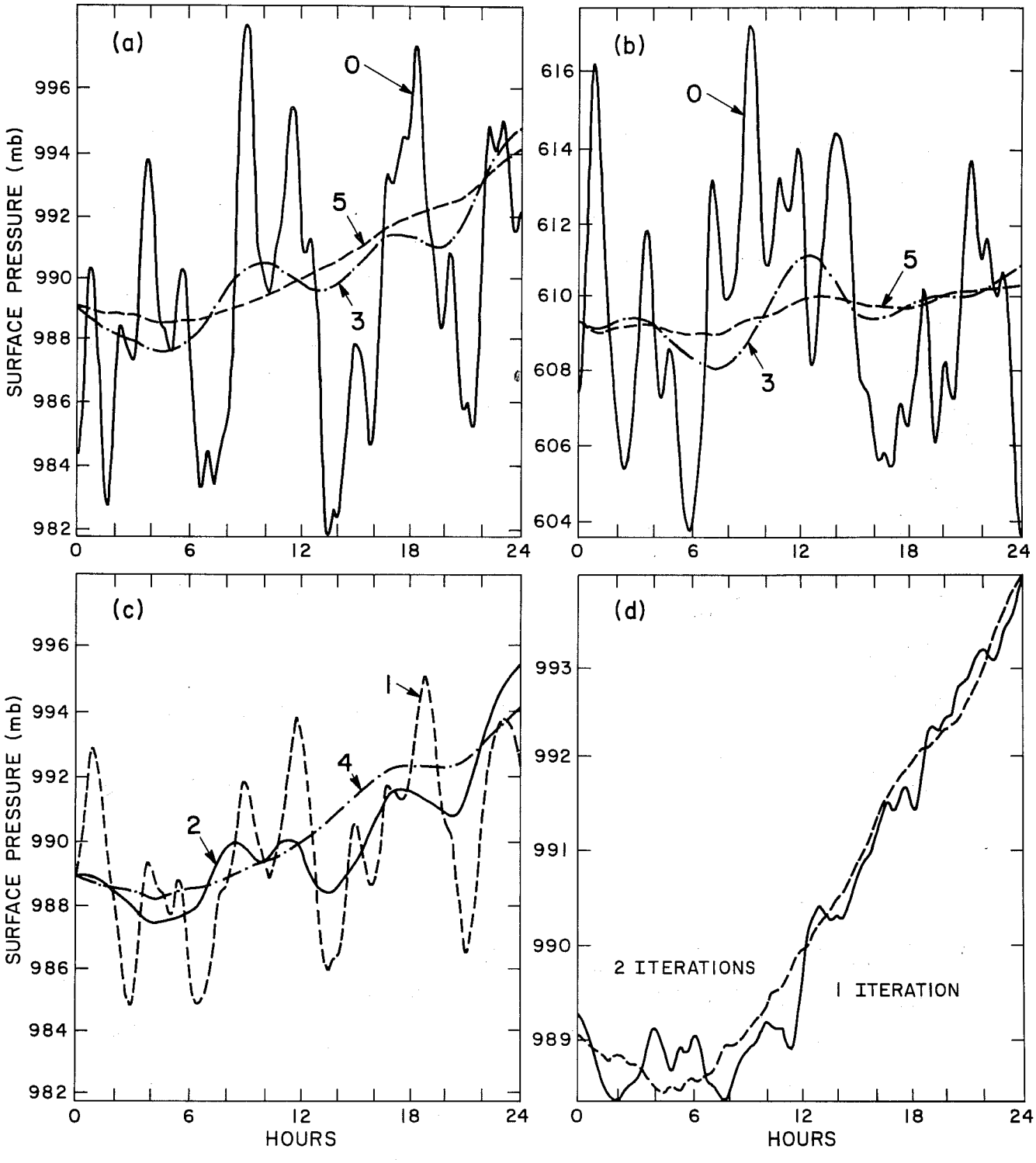

Fig. 5.2 Surface pressure vs time - (a) at 40 °N, 90 °W after two nonlinear iterations with the first three and five vertical modes and with no initialization, (b) as (a) but at 30 °N, 90 °E, (c) at 40 °N, 90 °W after two nonlinear iterations with the first one, two, and four vertical modes, and (d) at 40 °N, 90 °W after one and two nonlinear iterations with the first five vertical modes.

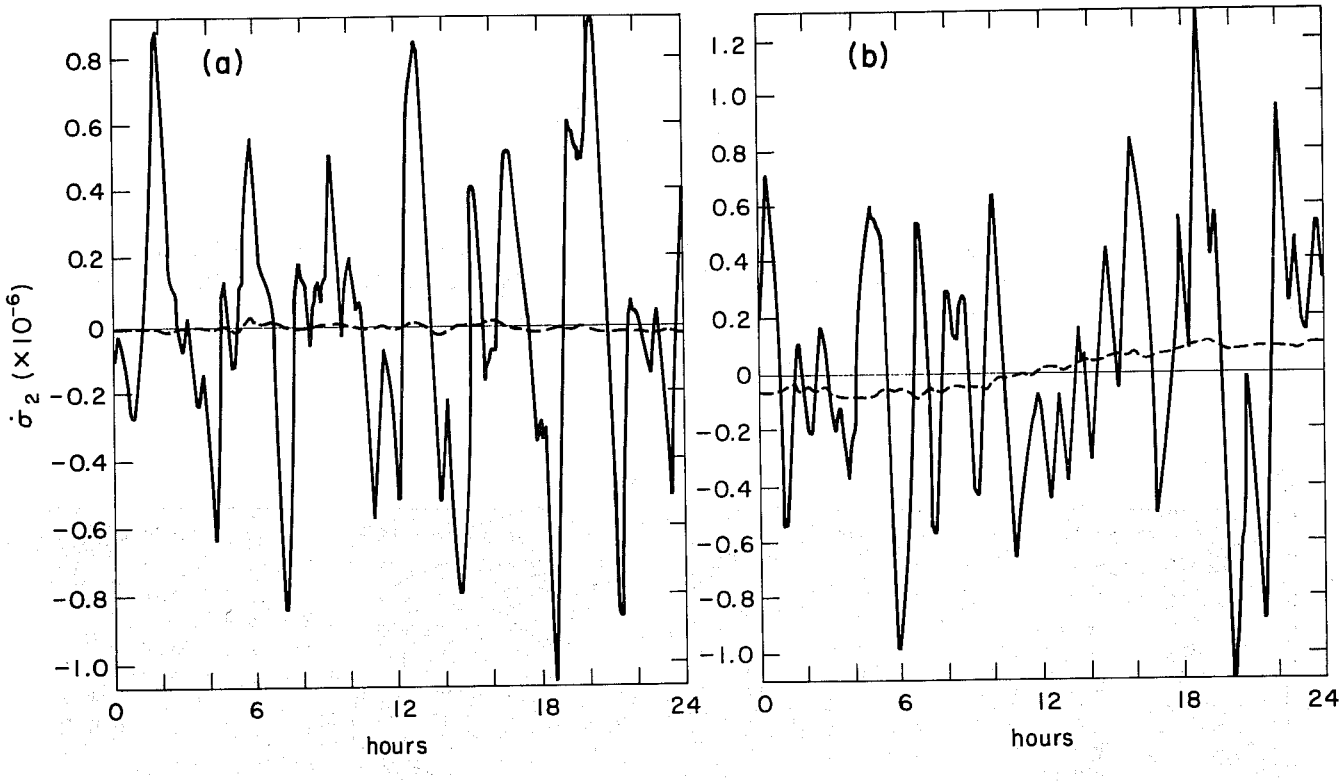

Fig. 5.3 $\dot{\sigma}$ vs. time at (a) 40 °N, 90 °W and (b) 30 °N, 90 °E with no initialization (solid line) and with two non-linear iterations with the first five vertical modes (dashed line).

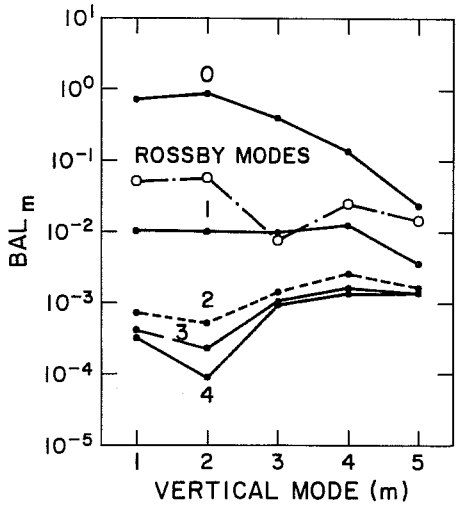

Fig. 5.4 Balance of symmetric gravity modes after one linear initialization followed by n nonlinear iterations on the first five vertical modes.

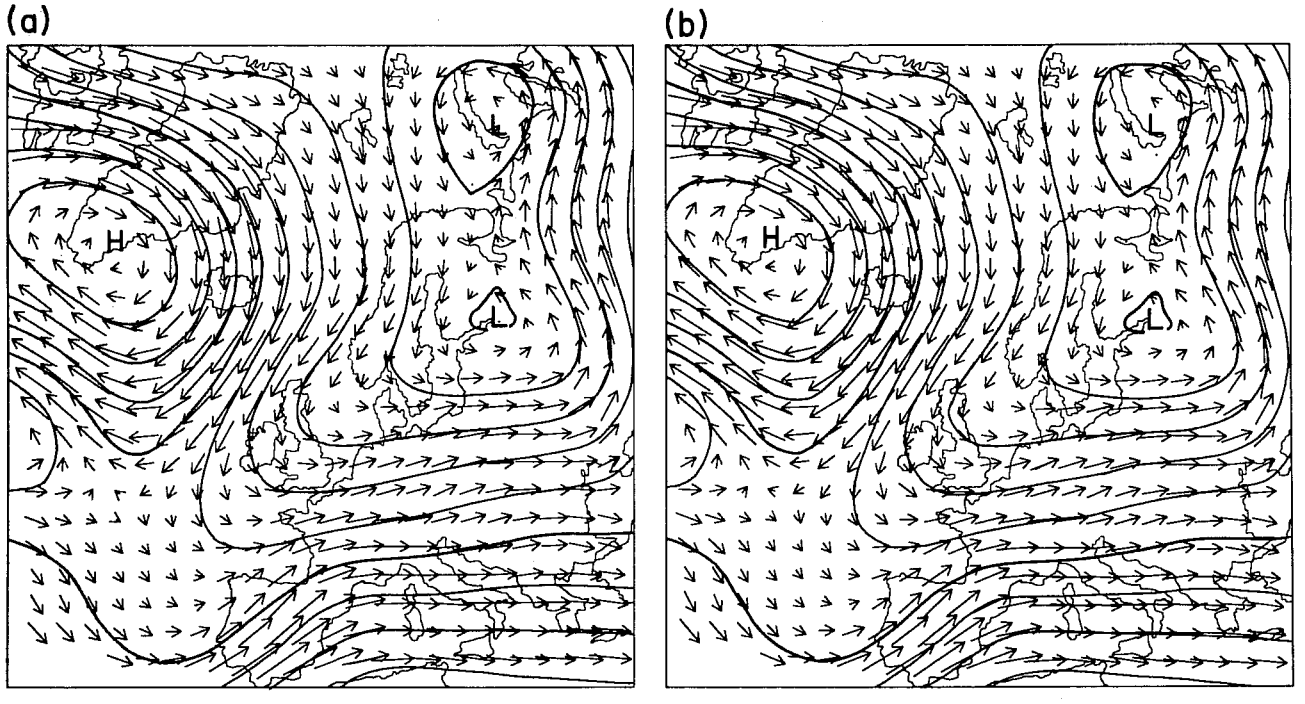

Fig. 5.5 (a) 500 mb height contour and wind vectors for linear initialization followed by two iterations of nonlinear initialization with the first five vertical modes,
(b) as (a) without the initial linear initialization.

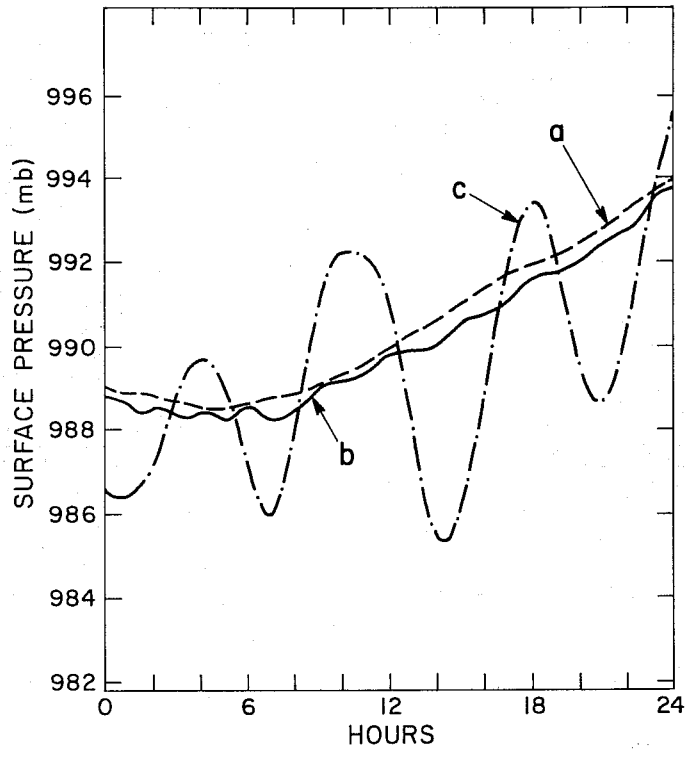

Fig. 5.6 Surface pressure vs time at 40 °N, 90 °W after (a) linear initialization followed by two nonlinear iterations of the first five vertical modes, (b) two nonlinear iterations of the first five vertical modes using vectors for $\overline{T}(\sigma)$ = 300K, (c) 6 h of dynamic initialization.

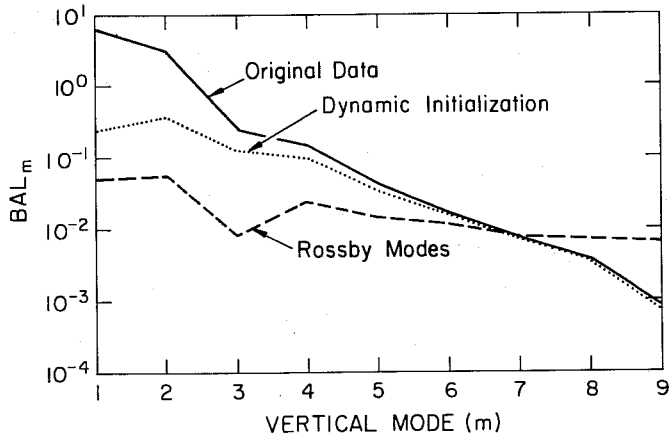

Fig. 5.7 Balance obtained by dynamic initialization.

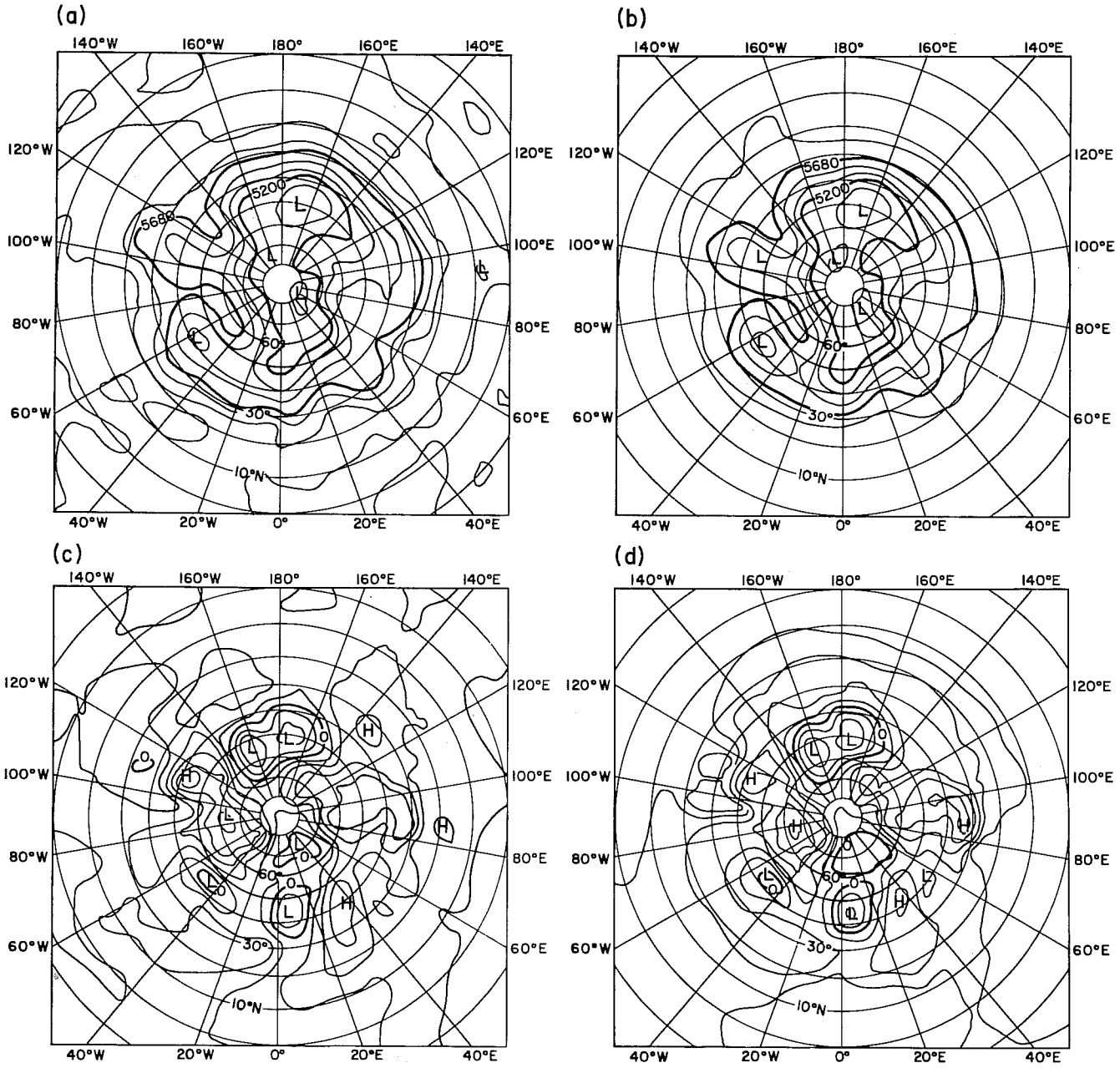

Fig. 5.8 24 h, 500 mb forecast after

(a) no initialization,
(b) two nonlinear iterations of the first five vertical modes;

and 24 h, 1000 mb forecast after

(c) no initialization,
(d) two nonlinear iterations of the first five vertical modes.

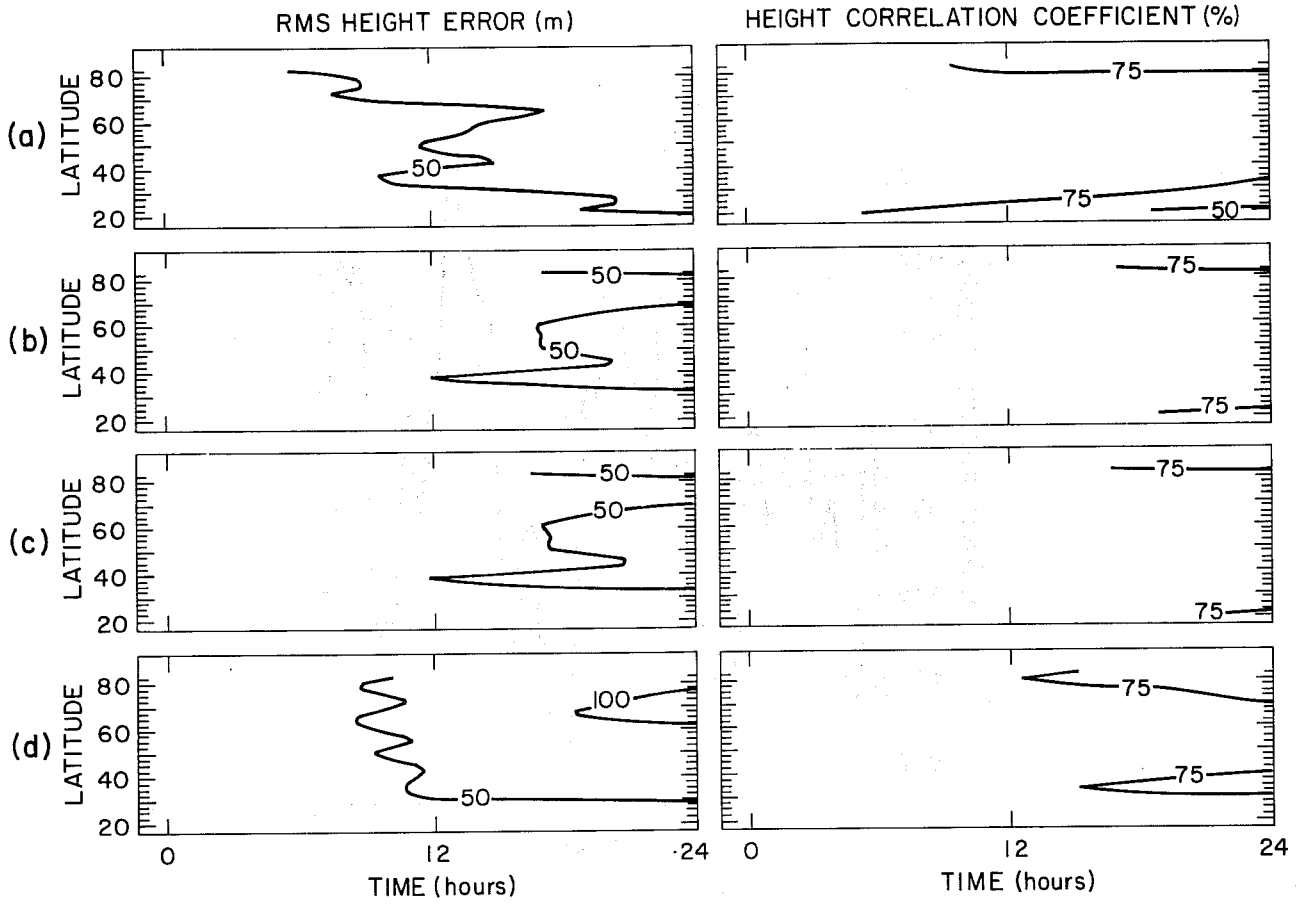

Fig. 5.9 Height RMS error and correlation coefficient as function of time and latitude - (a) uninitialized vs NMC, (b) initialized vs NMC, (c) uninitialized forecast followed by initialization vs NMC and (d) persistence vs NMC.

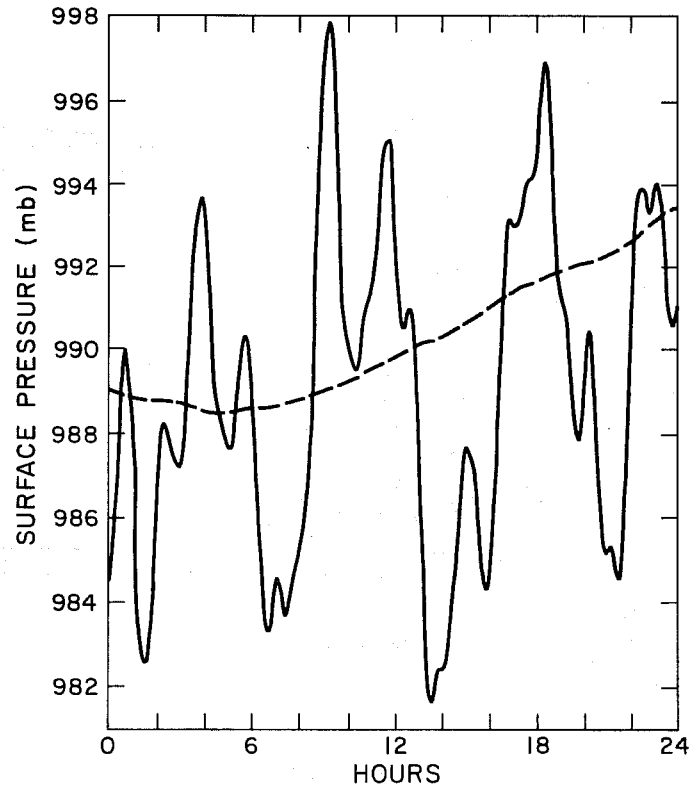

Fig. 6.1 Surface pressure vs time at 40 °N, 90 °W during forecast with friction, before (solid) and after (dashed) adiabatic nonlinear initialization (2 iterations, 5 vertical modes).

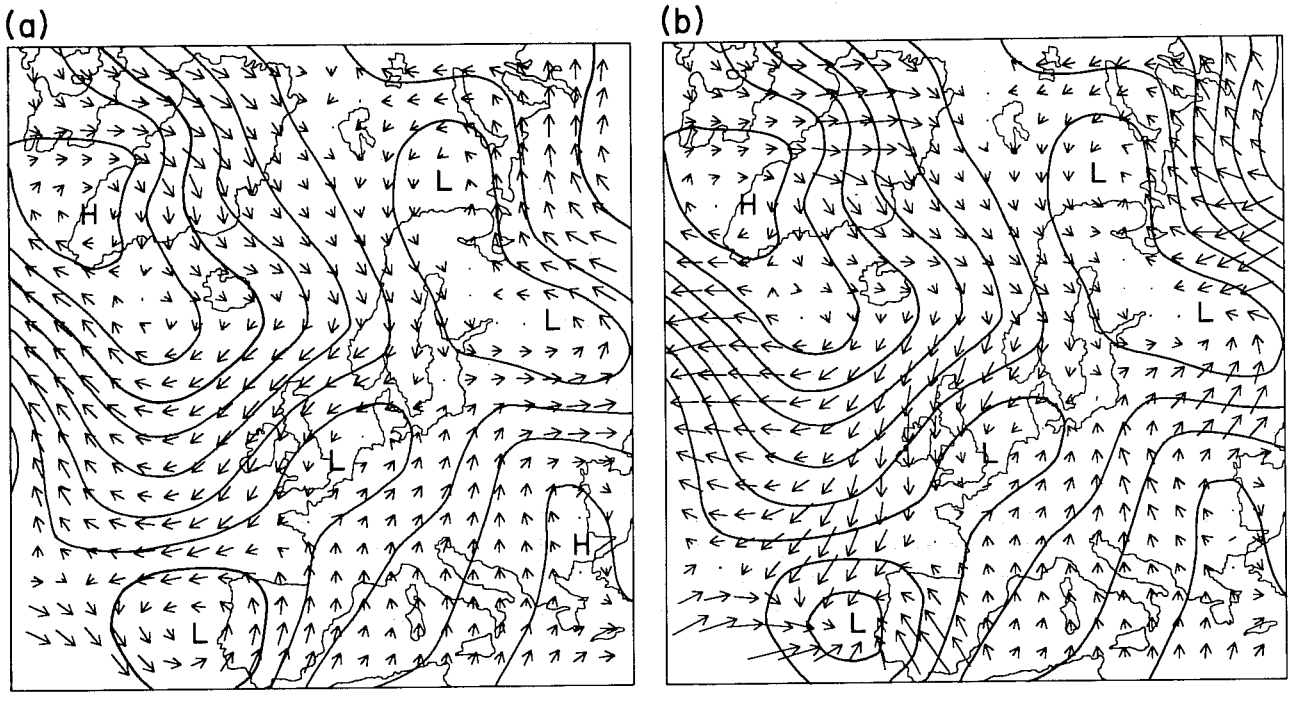

Fig. 6.2 1000 mb height field and lowest model level wind vectors after nonlinear initialization with friction
(a) 2 iterations with the first 5 vertical modes
(b) 1 iteration with 5 vertical modes followed by 1 iteration with 9.

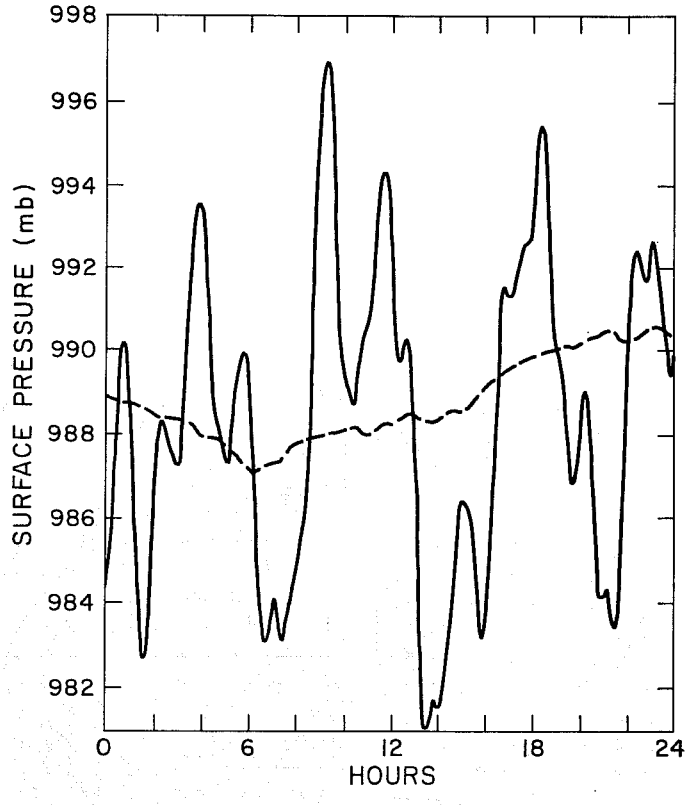

Fig. 6.3 Surface pressure vs time at 40 °N, 90 °W during forecasts with friction, before (solid) and after (dashed) nonlinear initialization with friction (2 iterations, first with 5 modes, then 9).

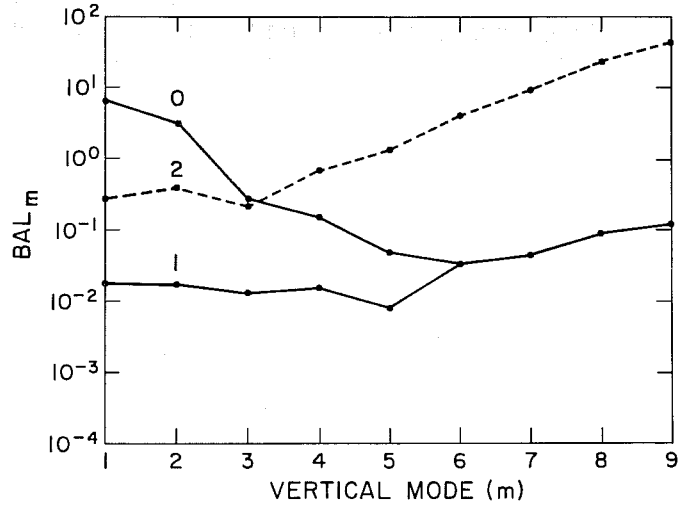

Fig. 6.4 Balance as measured by (5.7) of the symmetric gravity modes after one nonlinear iteration with friction and 5 vertical modes followed by an additional iteration with friction and 9 vertical modes.

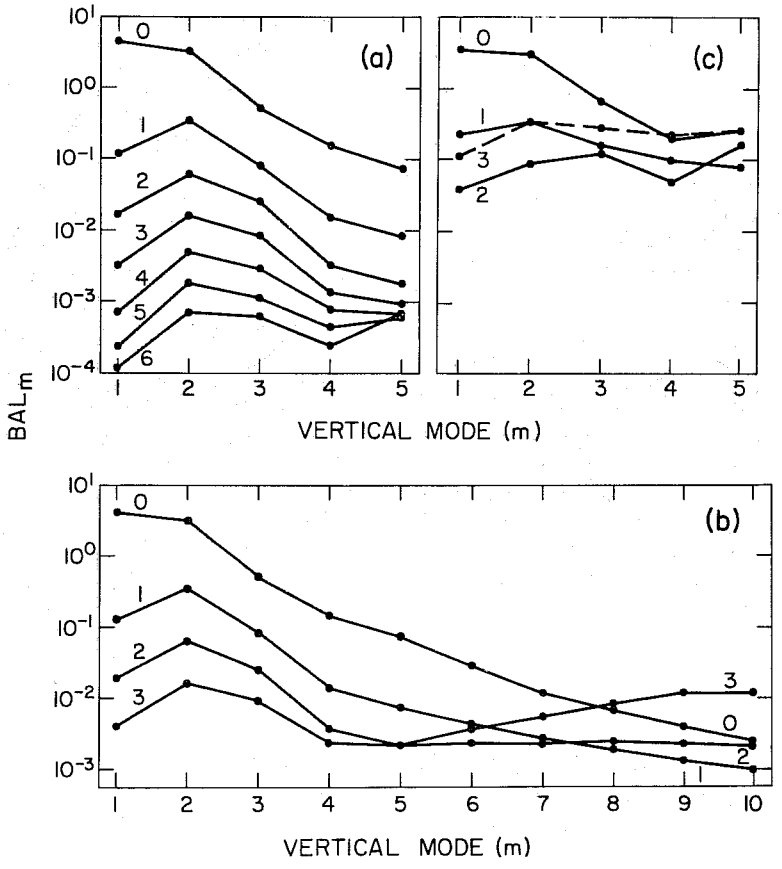

Fig. 7.1 Balance as measured by (5.7) of the symmetric gravity modes during nonlinear initialization for the 15-level N48 model: (a) 5 vertical modes, adiabatic; (b) 10 vertical modes, adiabatic; (c) 5 vertical modes, including physics package.

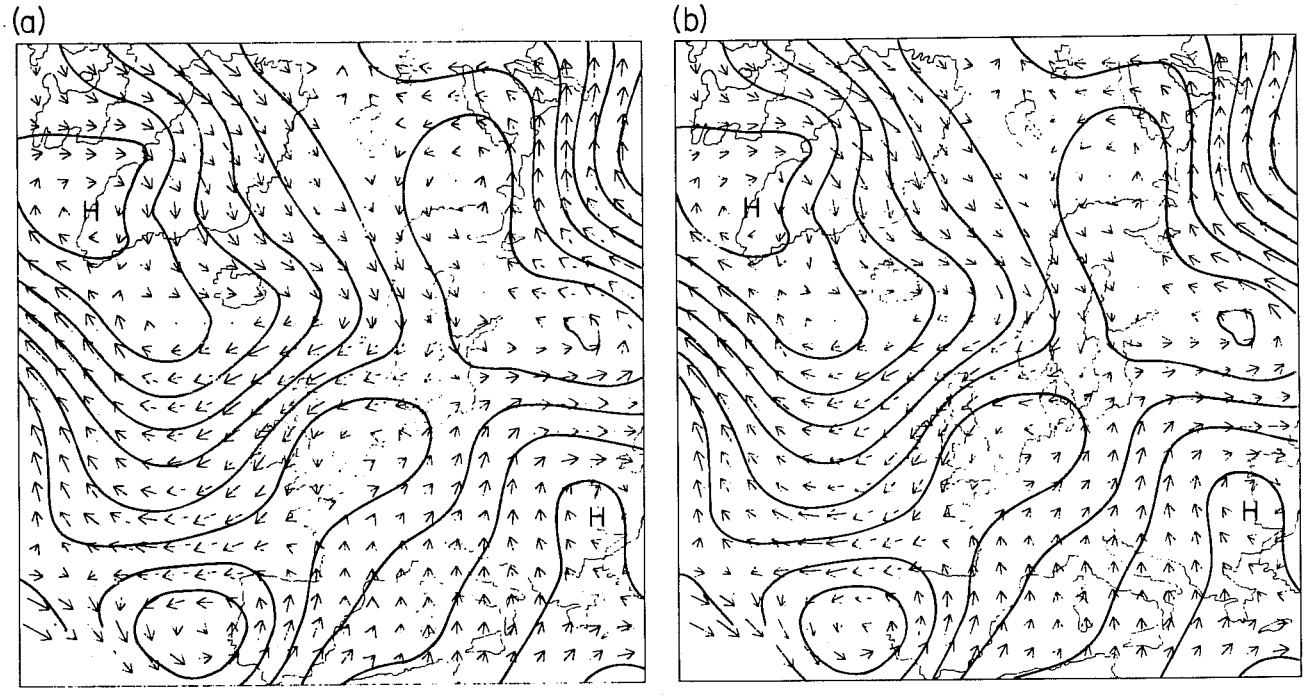

Fig. 7.2 1000 mb height and lowest model level winds after 2 iterations of nonlinear initialization, including 5 vertical modes: (a) adiabatic, (b) including physics package.

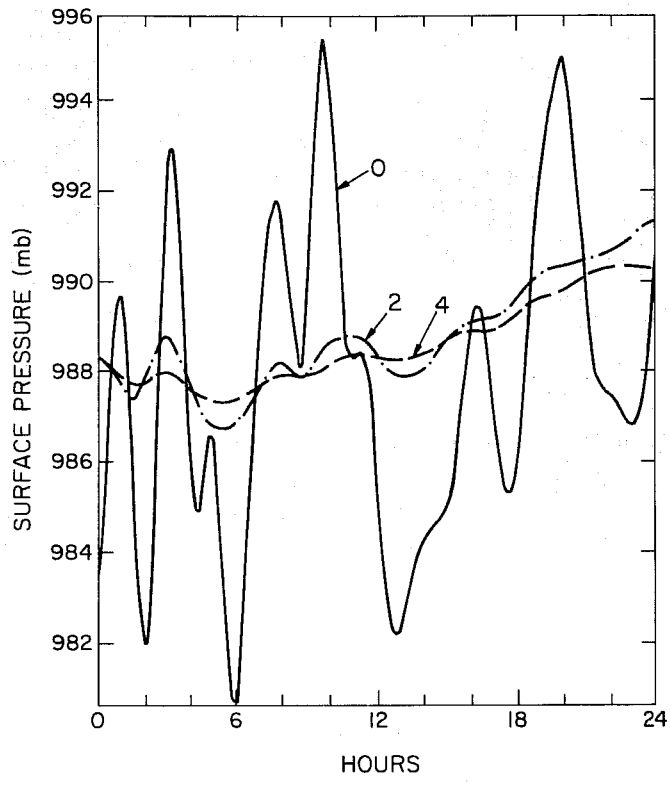

Fig. 7.3 Surface pressure vs time at 40 °N, 90 °W during forecasts with 15-level N48 model including physics package after no initialization and 2 and 4 iterations of nonlinear initialization (adiabatic, 5 vertical modes).

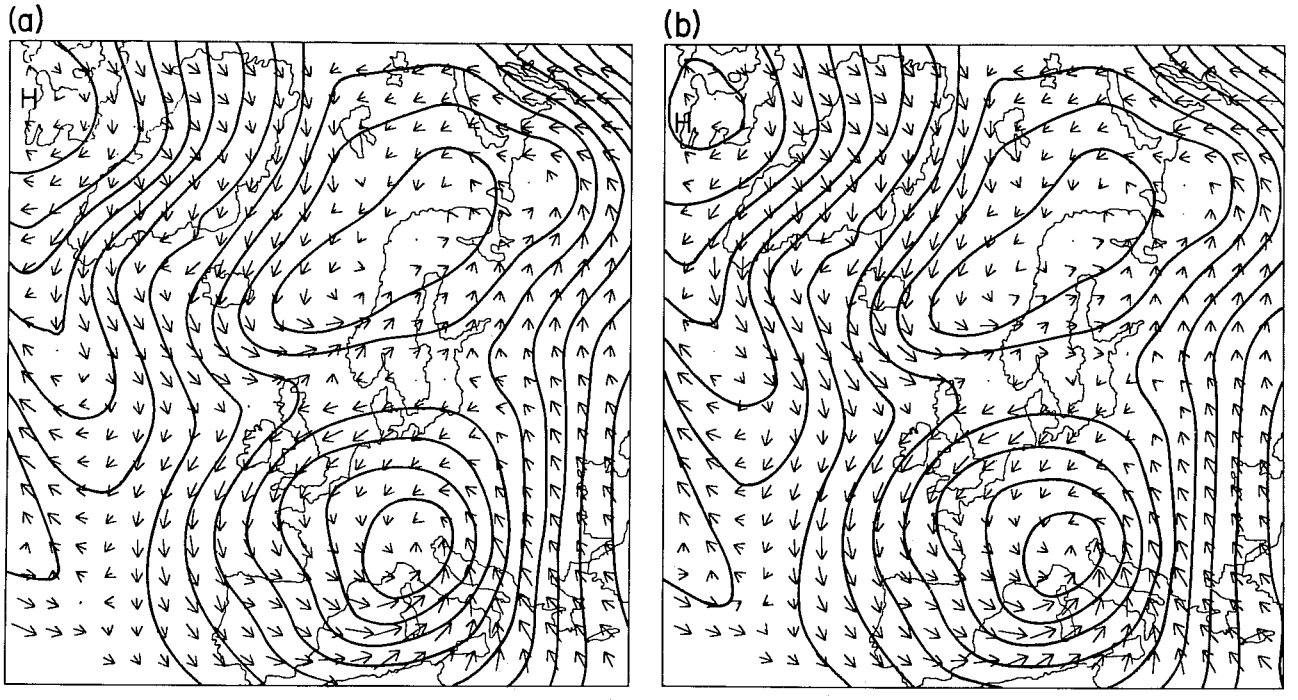

Fig. 7.4 1000 mb height and lowest model level winds from 24-hour forecast including physics package, (a) before and (b) after two iterations of nonlinear initialization (adiabatic, 5 vertical modes).

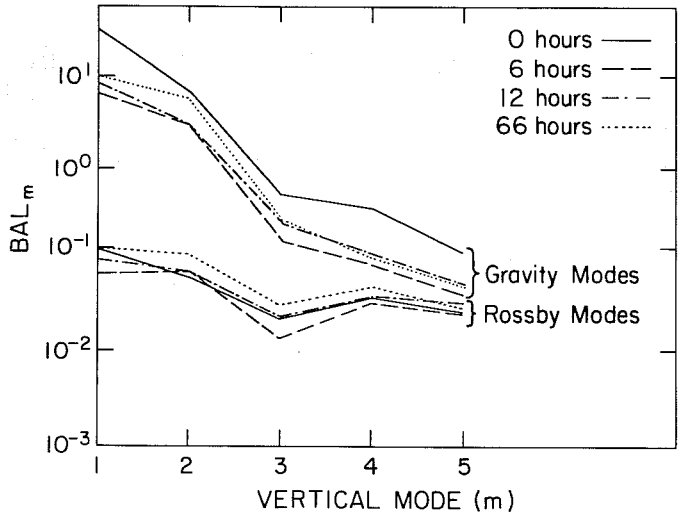

Fig. 8.1 Balance at various times in the analysis-forecast cycle.

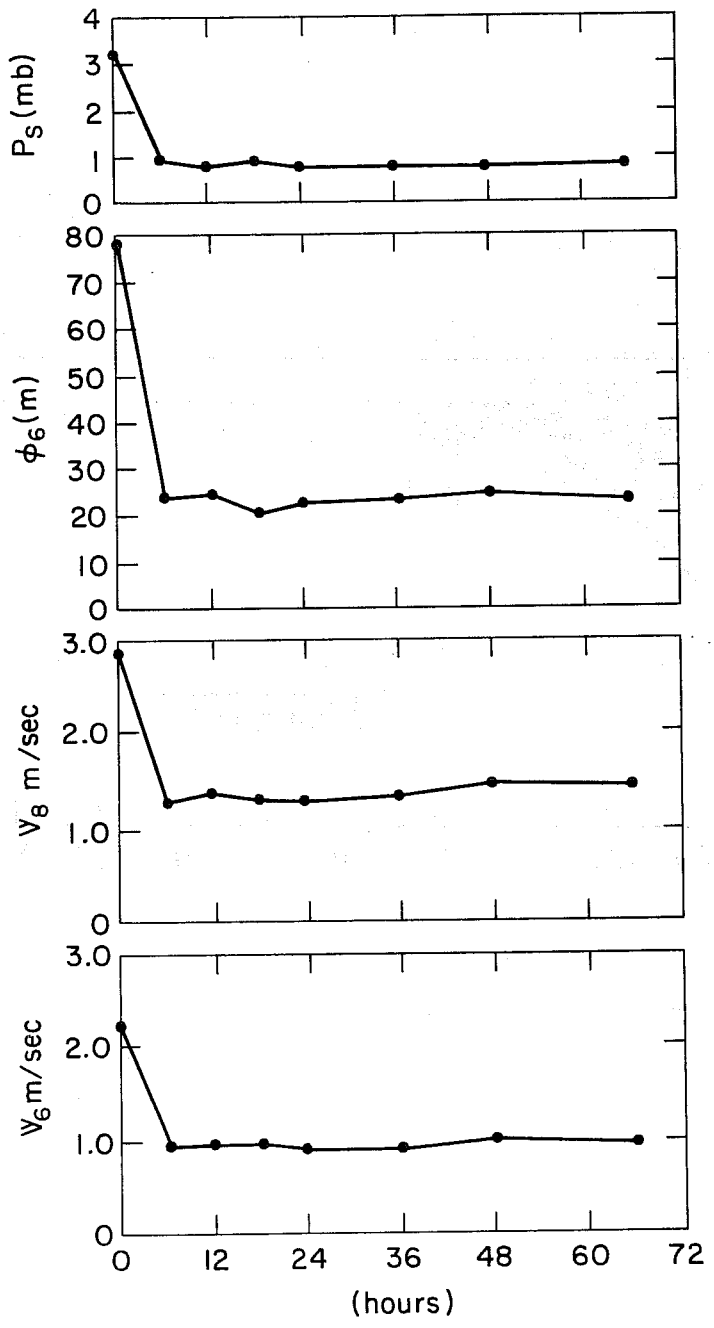

Fig. 8.2 RMS differences before and after initialization in the analysis-forecast cycle.

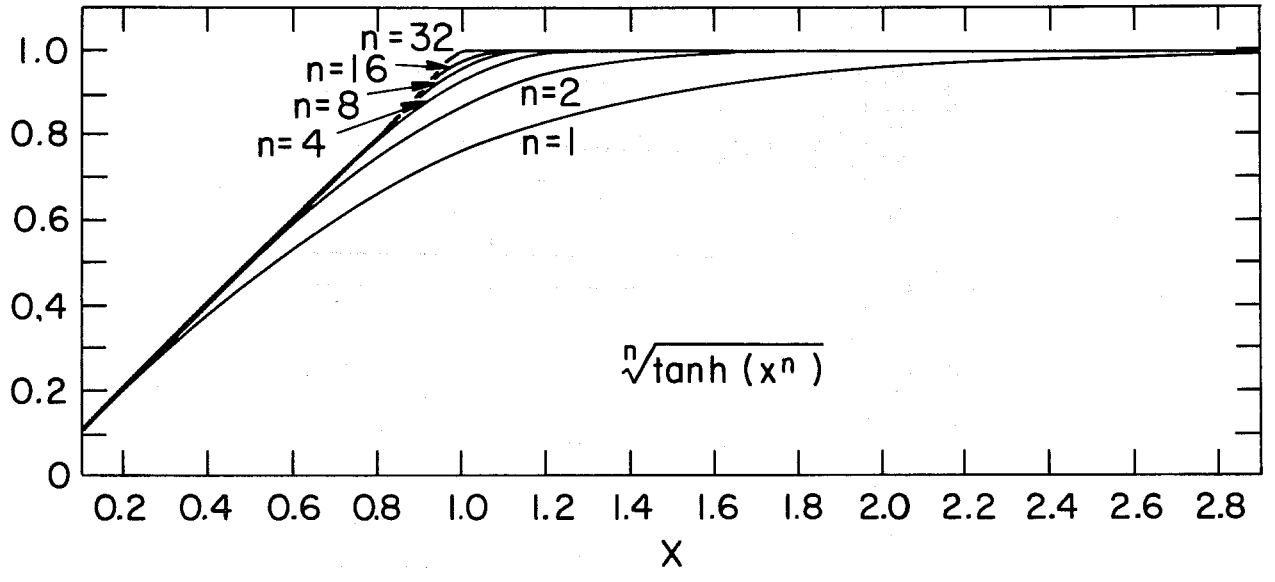

Fig. 8.3 The B^n function.

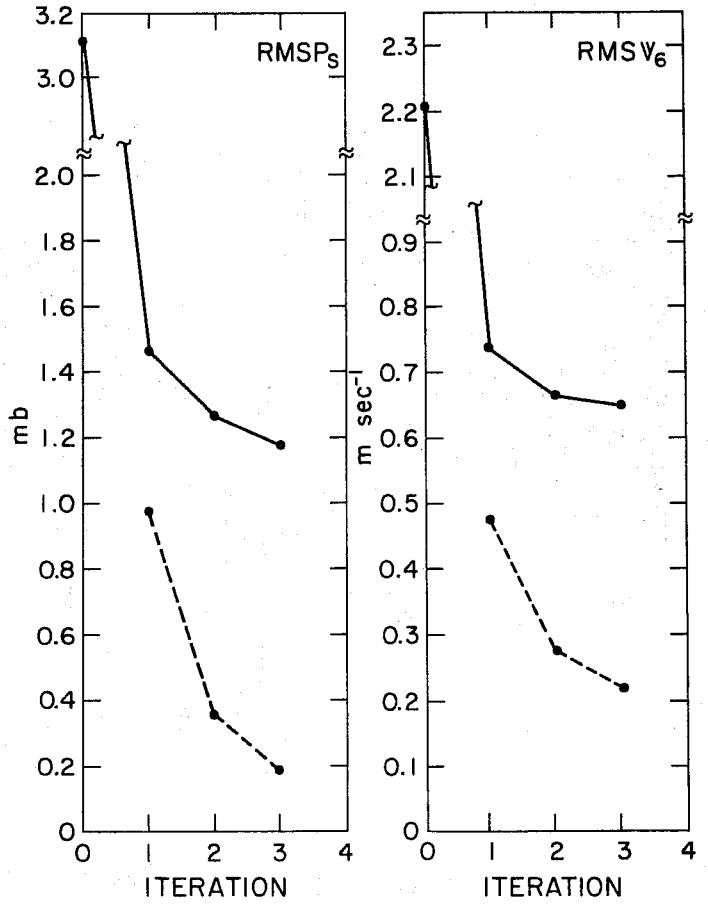

Fig. 8.4 RMS P_S and $\mathbb{V}_6$ differences during the forced adjustment. Upper curves represent differences caused by initialization, lower curves represent differences between successive initialized states.

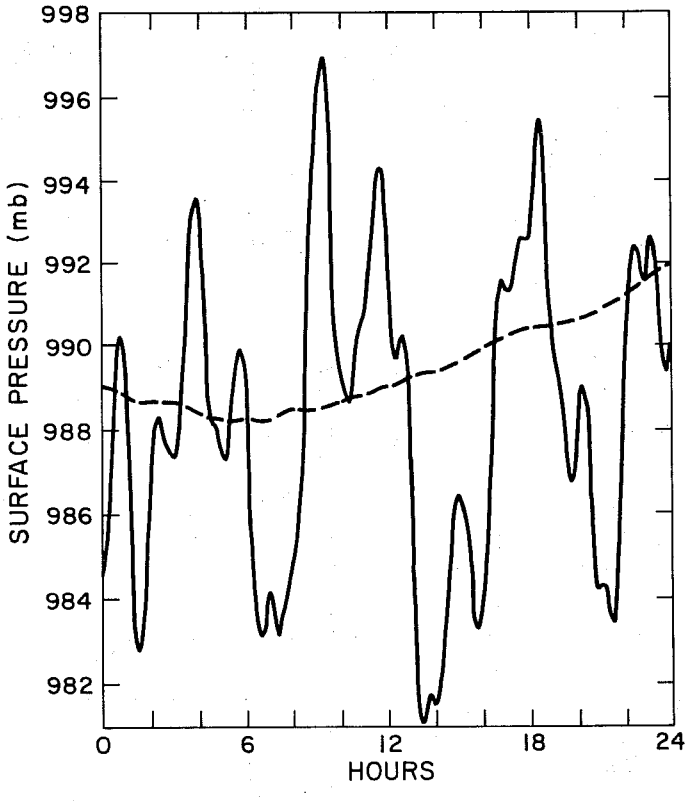

Fig. 9.1 Surface pressure vs time at 40 °N, 90 °W during forecasts with new Jacobian, before (solid) and after (dashed) nonlinear initialization (2 iterations, 5 vertical modes, using horizontal modes based on old Jacobian).

EUROPEAN CENTRE FOR MEDIUM RANGE WEATHER FORECASTS

Research Department (RD)

Technical Report No.11

No. 1 A Case Study of a Ten Day Prediction

No. 2 The Effect of Arithmetic Precision on some Meteorological Integrations

No. 3 Mixed-Radix Fast Fourier Transforms without Reordering

No. 4 A Model for Medium-Range Weather Forecasting -Adiabatic Formulation-

No. 5 A Study of some Parameterizations of Sub-Grid Processes in a Baroclinic Wave in a Two-Dimensional Model

No. 6 The ECMWF Analysis and Data Assimilation Scheme - Analysis of Mass and Wind Fields

No. 7 A Ten Day High Resolution Non-Adiabatic Spectral Integration : A Comparative Study

No. 8 On the Asymptotic Behaviour of simple Stochastic-Dynamic Systems

No. 9 On Balance Requirements as Initial Conditions

No.10 ECMWF Model - Parameterization of Sub-Grid Scale Processes

No.11 Normal Mode Initialisation for a multi-level Gridpoint Model

No.12 Data Assimilation Experiments

No.13 Comparison of medium range Forecasts made with two Parameterization Schemes

No.14 On Initial Conditions for Non-Hydrostatic Models